

Bayesian clustering of high-dimensional data via latent repulsive mixtures

Lorenzo Ghilotti¹, Mario Beraha², and Alessandra Guglielmi³

¹Department of Economics, Management and Statistics, University of Milano-Bicocca

²Department of Economics and Statistics, University of Torino

³Department of Mathematics, Politecnico di Milano

March 7, 2023

Abstract

Model-based clustering of moderate or large dimensional data is notoriously difficult. We propose a model for simultaneous dimensionality reduction and clustering by assuming a mixture model for a set of latent scores, which are then linked to the observations via a Gaussian latent factor model. This approach was recently investigated by Chandra et al. (2020). The authors use a factor-analytic representation and assume a mixture model for the latent factors. However, performance can deteriorate in the presence of model misspecification. Assuming a repulsive point process prior for the component-specific means of the mixture for the latent scores is shown to yield a more robust model that outperforms the standard mixture model for the latent factors in several simulated scenarios. To favor well-separated clusters of data, the repulsive point process must be anisotropic, and its density should be tractable for efficient posterior inference. We address these issues by proposing a general construction for anisotropic determinantal point processes.

KEYWORDS: Anisotropic point process; Determinantal point process; Gaussian factor model; MCMC; Model based clustering.

1 Introduction

This paper concerns Bayesian cluster analysis for moderate or high dimensional data. Specifically, we focus on observations $y_1, \dots, y_n \in \mathbb{R}^p$. Although a variety of models have been proposed in the literature (Neal, 2003; Teh et al., 2007; Duan & Dunson, 2021; Natarajan et al., 2021), Bayesian mixtures constitute a direct approach for model-based clustering; see Fruhwirth-Schnatter et al. (2019) for a recent review. In mixture models, it is assumed that data are generated from m (either random or fixed) homogeneous

populations. Typically, each population is assumed to be suitably modelled via a parametric density $f_\theta(\cdot)$ for some parameter $\theta \in \Theta$. Weights $\mathbf{w} = (w_1, \dots, w_m)$ ($w_h \geq 0$, $\sum_{h=1}^m w_h = 1$) specify the relative frequency of each population. In summary, the conditional distribution of data, given parameters, under the mixture model takes the form

$$y_1, \dots, y_n \mid \mathbf{w}, \boldsymbol{\theta} \stackrel{\text{iid}}{\sim} p(\cdot) = \sum_{h=1}^m w_h f_{\theta_h}(\cdot) \quad (1)$$

Under the Bayesian approach, suitable priors are assumed for \mathbf{w} , $\boldsymbol{\theta} = (\theta_1, \dots, \theta_m)$ and m .

The poor performance of Bayesian mixtures when p is larger than a moderate value, e.g. $p > 10$, is a long-standing issue. This is partly due to the poor scalability of the algorithms for posterior inference (see, e.g., Malsiner-Walli et al., 2016; Celeux et al., 2019), and partly due to the asymptotic properties of the model when p is large. Specifically, Theorem 1 together with Corollaries 1 and 2 in Chandra et al. (2020) shows the degeneracy of the cluster estimate when f_θ in (1) is the Gaussian distribution, that is, the de facto standard. As $p \rightarrow +\infty$, if the covariance matrix is cluster-specific, then with (posterior) probability one, all observations are clustered as singletons, while if the covariance matrix is shared among all the clusters, only one cluster is detected.

The most popular approach among practitioners to cluster high-dimensional data follows a two-step procedure: first, fitting a latent factor model (Lopes, 2014), a d -dimensional score η_i , where $d \ll p$, is associated with each observation. Then traditional clustering algorithms are applied to the η_i 's. However, this two-step procedure does not allow propagation of the variability induced by the dimensionality reduction step into the cluster estimates. To overcome this important limitation, the natural option is to consider a model for simultaneous dimensionality reduction and clustering, by assuming a mixture model for the latent scores, which are then linked to the observations via a Gaussian latent factor model. This approach was recently investigated by Chandra et al. (2020) within the Bayesian nonparametric framework.

However, mixture models might overestimate the number of clusters to recover the ‘‘true’’ sampling model. Indeed, the typical postulate in Bayesian mixture models is that parameters θ_h in (1) are i.i.d. from a base distribution. Under this assumption, if the true data generating density does not agree with (1), the number of clusters a posteriori diverges as n increases (Cai et al., 2021). Two sources of misspecification pertain to the Gaussian latent factor model with a standard mixture model for the latent scores: first, the factor-analytic representation entails that data lie close to a d -dimensional hyperplane; second, the deviation from such a hyperplane is Gaussian distributed. Both of these assumptions can be questioned and are unlikely to hold in practice. Moreover, Chandra et al. (2020) assume a Dirichlet process (DP) mixture prior for the latent scores which might yield inconsistent estimates even for well-specified models (Miller & Harrison, 2014). Promising results towards consistency of DP mixtures have been obtained in Ascolani et al. (2022), but their assumptions do not hold for the model in Chandra et al. (2020).

In the present paper, we propose APPLAM: Anisotropic (repulsive) Point Process Latent Mixture model. We consider a model for simultaneous dimensionality reduction and clustering as above, but assume a repulsive point process as the prior for the component-

specific location parameters of the mixture for the latent scores. Repulsive mixtures (Beraha et al., 2022) offer a practical solution to the lack of robustness of mixture models with i.i.d. component parameters. We argue that, in order to have well-separated clusters of data, it is not sufficient to have well-separated clusters at the latent level, but the repulsion should also take into account the factor analytic model that links the latent variables to the observations. To this end, we propose an anisotropic Determinantal point process (DPP) as the prior for the component-specific parameters, where the anisotropy is driven by the matrix of factor loadings. We derive a general construction of anisotropic DPPs that induce the desired repulsion. We develop novel existence conditions for our class of DPPs that are similar to those in Lavancier et al. (2015) and further provide an explicit expression for the spectral density of the DPP, which is essential for simulation purposes. Moreover, we design an efficient block Gibbs sampler for posterior simulations.

2 Methodology

2.1 Bayesian clustering via latent mixtures

Let $\mathbf{y} = (y_1, \dots, y_n)$, $y_i \in \mathbb{R}^p$, $\Lambda \in \mathbb{R}^{p \times d}$ be the matrix of factor loadings, $\eta_1, \dots, \eta_m \in \mathbb{R}^d$ be a set of latent factors, and $\Sigma = \text{diag}(\sigma_1^2, \dots, \sigma_p^2)$ ($\sigma_j > 0$) be a diagonal covariance matrix. Let $\mathcal{N}_p(\mathbf{a}, B)$ denote the p -dimensional Gaussian distribution with mean \mathbf{a} and covariance matrix B . We assume

$$\begin{aligned} y_i | \eta_i, \Lambda, \Sigma &\stackrel{\text{ind}}{\sim} \mathcal{N}_p(\Lambda \eta_i, \Sigma), \\ \eta_i | \mathbf{w}, \boldsymbol{\mu}, \boldsymbol{\Delta} &\stackrel{\text{iid}}{\sim} \sum_{h=1}^m w_h \mathcal{N}_d(\mu_h, \Delta_h), \end{aligned} \quad (2)$$

for $i = 1, \dots, n$. Extensions to other kernel distributions for the mixture model for latent factors and for observations are straightforward. The prior for $\mathbf{w} = (w_1, \dots, w_m)$, $\boldsymbol{\mu} = (\mu_1, \dots, \mu_m)$, $\boldsymbol{\Delta} = (\Delta_1, \dots, \Delta_m)$, m , Λ , and the σ_j^2 's will be specified in Section 2.3 below.

Introducing a set of latent cluster indicator variables c_i such that $P(c_i = h | \mathbf{w}) = w_h$, we can equivalently state the prior for the η_i 's in (2) as

$$\eta_i | c_i = h, \boldsymbol{\mu}, \boldsymbol{\Delta} \stackrel{\text{ind}}{\sim} \mathcal{N}_d(\mu_h, \Delta_h), \quad i = 1, \dots, n. \quad (3)$$

Therefore, as is standard in Bayesian mixture models, we cluster data y_i 's through the latent variables η_i 's, i.e., y_i and y_j belong to the same cluster if $c_i = c_j$. Through the c_i 's we can identify the clusters with the allocated components, i.e. those components $h \in \{1, \dots, m\}$ for which there exists i such that $c_i = h$.

The cluster estimate is interpretable and hence useful if observations belonging to different clusters are well separated. Repulsive mixture models encourage well-separated clusters by assuming a prior for the cluster centers that favors regular (i.e., well-separated) point configurations. A straightforward approach to define such a prior is assuming a repulsive point process which governs both the cardinality m of the components and the

locations of the μ_h 's. In particular, it is possible to define such a process by specifying a density with respect to a Poisson point process. For instance, Quinlan et al. (2020); Xie & Xu (2019); Beraha et al. (2022) assume a pairwise interaction process whose density, with respect to a suitably defined Poisson process, is

$$p(\{\mu_1, \dots, \mu_m\}) = \frac{1}{Z} \prod_{j=1}^m \phi_1(\mu_j) \prod_{1 \leq h < k \leq m} \phi_2(\|\mu_h - \mu_k\|) \quad (4)$$

where ϕ_1 is a bounded function, ϕ_2 is a non-decreasing function, and Z is a normalization constant that is usually intractable. See Daley & Vere-Jones (2008) and Møller & Waagepetersen (2003) for the definition of density with respect to a Poisson point process.

This choice of the prior would ensure that different clusters are associated with well-separated latent scores η_i 's, but is this enough to ensure well-separated clusters of data y_i 's? By the properties of the Gaussian distribution, we have

$$\{y_i : c_i = h\} \mid \mathbf{c}, \boldsymbol{\mu}, \boldsymbol{\Delta}, \boldsymbol{\Lambda} \stackrel{\text{iid}}{\sim} \mathcal{N}_p(\boldsymbol{\Lambda}\mu_h, \boldsymbol{\Lambda}\boldsymbol{\Delta}_h\boldsymbol{\Lambda}^\top + \boldsymbol{\Sigma}).$$

Hence, it is clear that it is not sufficient to encourage a priori that $\|\mu_h - \mu_k\|$ is large to obtain well separated clusters of datapoints, as the distance between cluster centers is $\|\boldsymbol{\Lambda}\mu_h - \boldsymbol{\Lambda}\mu_k\|$. To this end, we could easily modify (4) by considering $\phi_2(x) \equiv \tilde{\phi}_2(\|\boldsymbol{\Lambda}x\|)$, where now the normalizing constant Z depends on ϕ_1, ϕ_2 and, most importantly, $\boldsymbol{\Lambda}$. The intractability of the normalizing constant in (4) poses a significant challenge to posterior simulation. Beraha et al. (2022) discuss how to sample from the posterior distribution of the parameters involved in (4) using the exchange algorithm (Møller et al., 2006; Murray et al., 2006), which requires perfect sampling from (4). However Beraha et al. (2022) investigate the efficiency of the algorithm only when sampling a single real-valued parameter. Here, instead, the point process density does depend on $\boldsymbol{\Lambda}$ and our preliminary investigation showed that updating $\boldsymbol{\Lambda}$ via the exchange algorithm results in extremely poor mixing due to the high-dimensionality of the matrix $\boldsymbol{\Lambda}$ itself.

In the rest of the paper, we propose a prior for the cluster centers $\{\mu_1, \dots, \mu_h\}$ based on a novel construction for anisotropic determinantal point processes, defined in the next section, whose density does not involve intractable terms. This allows us to use the well known Metropolis adjusted Langevin algorithm when sampling from the full conditional of $\boldsymbol{\Lambda}$, leading to better MCMC mixing even when p is large. Furthermore, we provide an analytical expression for the gradient of (the logarithm of) the DPP density with respect to $\boldsymbol{\Lambda}$ and show that it is cheap to compute when compared to gradients computed via automatic differentiation algorithms.

2.2 A general construction for anisotropic DPPs

Let Φ be a point process on $(\mathbb{R}^d, \mathcal{B}(\mathbb{R}^d))$. We consider Φ as a random point configuration $\Phi \equiv \{\mu_1, \dots, \mu_m\} \subset \mathbb{R}^d$ or as a random counting measure $\Phi(B) = \sum_{\mu_j \in \Phi} \mathbb{1}[\mu_j \in B]$ depending on the convenience. Determinantal point processes (DPPs) are usually defined in terms of their m -th factorial moment measures (Macchi, 1975; Lavancier et al., 2015;

Baccelli et al., 2020). Briefly, the m -th factorial measure of Φ is defined as

$$\Phi^{(m)}(B_1 \times \cdots \times B_m) = \sum_{\substack{\neq \\ \mu_1, \dots, \mu_m \in \Phi}} \mathbb{1}[\mu_1 \in B_1] \cdots \mathbb{1}[\mu_m \in B_m]$$

for measurable $B_1, \dots, B_m \subset \mathbb{R}^d$. The summation is intended over all m -tuples of pairwise different points in Φ . The m -th factorial moment measure is defined as $M_{\Phi^{(m)}}(B_1 \times \cdots \times B_m) = \mathbb{E} [\Phi^{(m)}(B_1 \times \cdots \times B_m)]$, where the expectation is taken with respect to Φ .

In order to define a DPP, let $K : \mathbb{R}^d \times \mathbb{R}^d \rightarrow \mathbb{C}$ be a continuous covariance kernel. Then Φ is a DPP on \mathbb{R}^d if, for all $m = 1, 2, \dots$, its m -th factorial moment measure has a density, with respect to the m -folded product of the d -dimensional Lebesgue measure, $\rho^{(m)}$, defined as

$$\rho^{(m)}(\mu_1, \dots, \mu_m) = \det\{K(\mu_h, \mu_k)\}_{h,k=1,\dots,m}, \quad \mu_1, \dots, \mu_m \in \mathbb{R}^d.$$

By Mercer's theorem $K(x, y) = \sum_{j \geq 1} \gamma_j \xi_j(x) \bar{\xi}_j(y)$ where the ξ_j 's form an orthonormal basis for $L^2(\mathbb{R}^d; \mathbb{C})$ of complex-valued functions and the γ_j 's are a summable nonnegative sequence. Then, existence of a DPP with kernel K is equivalent to $\gamma_j \leq 1$ for all j , see Macchi (1975). When restricted to a compact $R \subset \mathbb{R}^d$, Φ is still a DPP with kernel K restricted to $R \times R$. In particular, if $\gamma_j < 1$ for all j , Φ has a density with respect to the unit rate Poisson point process on R given by

$$p(\{\mu_1, \dots, \mu_m\}) = e^{|R|^{-D}} \det\{C(\mu_h, \mu_k)\}_{h,k=1,\dots,m}, \quad \mu_1, \dots, \mu_m \in R. \quad (5)$$

where $C(x, y) = \sum_{j \geq 1} \gamma_j / (1 - \gamma_j) \xi_j(x) \bar{\xi}_j(y)$, $|R| = \int_R dx$, and $D = -\sum_{j \geq 1} \log(1 - \gamma_j)$. See Lavancier et al. (2015) for a proof of such results.

Analytic expressions for γ_j are crucial for inferential purposes. Following the so-called ‘‘spectral approach’’ by Lavancier et al. (2015), Bianchini et al. (2020) and Beraha et al. (2022) assume $K(x, y) = K_0(x - y) = K_0(\|x - y\|)$, i.e., K is a stationary and isotropic function. Instead of modeling K , they fix the ξ_j 's as the Fourier basis and assume a parametric model for the γ_j 's. This approach ensures the positive definiteness of K and the existence of the DPP density, but is not flexible enough for the mixture model (2). In particular, isotropy of the DPP kernel K conflicts with our goal of forcing repulsion across the $\Lambda\mu_h$'s. In the following, we provide a general construction for stationary anisotropic DPPs, providing explicit expression for the Fourier transform of its kernel K_0 , and easy-to-check conditions that guarantee the existence of the DPP.

Theorem 2.1. *Let Λ be a (fixed) $p \times d$ real matrix with full rank. Let W be a strictly positive random variable and let $h(y)$ be the marginal density of the random variable Y defined as*

$$Y | W \sim \mathcal{N}_d(0, W(\Lambda^T \Lambda)^{-1}) \quad (6)$$

Let $K_0(x) = \rho h(x) / h(0)$ for $x \in \mathbb{R}^d$ and $\rho > 0$. Then there exists a DPP Φ on \mathbb{R}^d with kernel $K(x, y) = K_0(x - y)$ for $\rho \leq \rho_{\max}$ defined as

$$\rho_{\max} = |\Lambda^T \Lambda|^{\frac{1}{2}} (2\pi)^{-d/2} \mathbb{E}[W^{-\frac{d}{2}}], \quad (7)$$

and

$$K_0(x) = \frac{\rho}{\mathbb{E}[W^{-\frac{d}{2}}]} \mathbb{E}\left[W^{-\frac{d}{2}} \exp\left(-\frac{\|\Lambda x\|^2}{2W}\right)\right], \quad x \in \mathbb{R}^d. \quad (8)$$

If $\varphi(x) = \mathcal{F}(K_0)(x)$ denotes the Fourier transform of K_0 , we have that

$$\varphi(x) = \frac{\rho}{h(0)} \mathbb{E}[\exp(-2\pi^2 W x^T (\Lambda^T \Lambda)^{-1} x)], \quad x \in \mathbb{R}^d \quad (9)$$

Moreover, for any compact $R \subset \mathbb{R}^d$, the restriction of Φ to R has density with respect to the unit rate Poisson point process on R if $\rho < \rho_{\max}$.

Parameter ρ in Theorem 2.1 is the intensity of the process, i.e. it controls the distribution of the number of points in the process. In particular, the expected total number of points in R is equal to ρ . Let us remark that explicit knowledge of the Fourier transform is essential for simulation purposes, as one typically approximates the density of the DPP using φ as described in Section 3.1. In the following, we will use notation $\Phi \sim \text{DPP}(\rho, \Lambda, K_0; R)$ to denote the law of a DPP on R with intensity ρ , stationary kernel K_0 and anisotropy driven by Λ . Although the intensity ρ and the $p \times d$ matrix Λ appear implicitly in the definition of K_0 , we make them explicit in our notation to stress the importance of the parameters ρ and Λ .

The following result is an equivalent characterization of $\Phi \sim \text{DPP}(\rho, \Lambda, K_0; R)$.

Theorem 2.2. *Let $\Phi \sim \text{DPP}(\rho, \Lambda, K_0; R)$, then $\tilde{\Phi} = \{\Lambda\mu : \mu \in \Phi\}$ is a stationary and isotropic DPP on $B = \Lambda\mathbb{R}^d$. Specifically, its m -th factorial moment measure has a density with respect to the m -folded product of the Lebesgue measure on B defined as*

$$\det\{\tilde{K}_0(\|\tilde{\mu}_h - \tilde{\mu}_k\|)\}_{h,k=1,\dots,m} \quad \tilde{\mu}_1, \dots, \tilde{\mu}_m \in B$$

where

$$\tilde{K}_0(y) = \frac{\rho \det(\Lambda^T \Lambda)^{-1/2}}{\mathbb{E}[W^{-d/2}]} \mathbb{E}\left[W^{-d/2} e^{-\|y\|^2/2}\right]$$

Theorem 2.2 shows that our definition of anisotropic DPP is indeed equivalent to assuming an isotropic DPP in the high-dimensional space spanned by the columns of Λ , which ensures that the cluster centers $\Lambda\mu_h$'s are well separated. Nonetheless, the characterization in Theorem 2.2 is more operational, since assuming Λ random, as we do in the rest of the paper, can be easily done using the definition in Theorem 2.1. Instead, the approach as in Theorem 2.2 implies the need of computing the eigendecomposition of \tilde{K}_0 on a random hyperplane, which is a challenging task.

The type or strength of repulsion is controlled by the random variable $W \sim p(w)$ in Theorem 2.1. In the rest of the paper, we consider one specific choice for the random variable W in Theorem 2.1, leading to the anisotropic counterpart of the Gaussian DPPs discussed in Lavancier et al. (2015), which we refer to as Gaussian-like DPP in the following. Moreover, to prove the generality of our approach, in Appendix C we show how to construct an anisotropic counterpart of the Whittle-Matérn DPP, although we will not use it in our examples.

Corollary 2.3. *Using the same notation of Theorem 2.1, let W be a degenerate random variable defined as $W = |\Lambda^T \Lambda|^{\frac{1}{d}} c^{-2/d}$, for $c > 0$, where Λ is fixed. Then the kernel K_0 , its Fourier transform $\varphi = \mathcal{F}(K_0)$ and ρ_{\max} follow here:*

$$\begin{aligned} K_0(x) &= \rho \exp\left(-\frac{\|\Lambda x\|^2}{2|\Lambda^T \Lambda|^{\frac{1}{d}} c^{-\frac{2}{d}}}\right), & x \in \mathbb{R}^d \\ \varphi(x) &= \rho \frac{(2\pi)^{2/d}}{c} \exp\left(-2\pi^2 |\Lambda^T \Lambda|^{\frac{1}{d}} c^{-\frac{2}{d}} x^T (\Lambda^T \Lambda)^{-1} x\right), & x \in \mathbb{R}^d \\ \rho_{\max} &= c(2\pi)^{-d/2}. \end{aligned} \quad (10)$$

We conclude this section by investigating the effect that Λ has on the repulsiveness of the DPP. First of all, it is clear that Λ induces anisotropy. To visualize this, we consider the pair correlation function $g(x)$ (PCF, Lavancier et al., 2015); for the Gaussian-like DPP:

$$g(x) = 1 - \frac{K_0(x)}{K_0(0)} = 1 - \exp\left(-\frac{\|\Lambda x\|^2}{2|\Lambda^T \Lambda|^{\frac{1}{d}} c^{-\frac{2}{d}}}\right)^2, \quad x \in \mathbb{R}^d$$

and set $p = d = 2$ for visual purposes. Figure 1 shows the PCFs of two Gaussian-like DPPs with different $\Lambda \in \mathbb{R}^{2 \times 2}$. In the left panel, Λ has eigenvectors $e_1 = (1, 0)^T$, $e_2 = (0, 1)^T$ and eigenvalues $\lambda_1 = 1$, $\lambda_2 = \lambda$, which induces stronger repulsion along the horizontal axis than along the vertical one. In the right panel, Λ has eigenvectors $e_1 = \sqrt{2}/2(1, 1)^T$, $e_2 = \sqrt{2}/2(-1, 1)^T$ and eigenvalues $\lambda_1 = 1$, $\lambda_2 = \lambda$, which induces stronger repulsion along the bisector of the first quadrant than along the orthogonal direction.

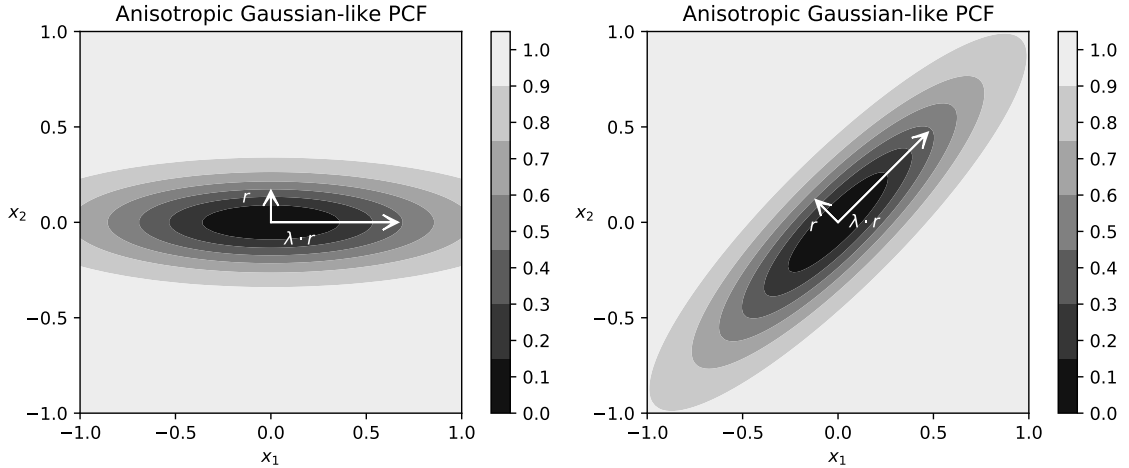


Figure 1: Pair correlation function of two Gaussian-like DPPs, one showing strong repulsion along the horizontal direction (left plot) and one showing strong repulsion along the bisector of the first quadrant (right plot).

Although the PCF is useful for visualizing the anisotropy of repulsiveness, it provides little information on *how much* repulsiveness is induced by the DPP. Several repulsiveness measures have been proposed for spatial point processes. See, e.g., Lavancier et al.

(2015); Biscio & Lavancier (2016) for a few quantitative indexes of global and local repulsiveness. Here, we focus in particular on the coefficient p_0 introduced in Møller & O'Reilly (2021) that is derived from a coupling between the DPP and its reduced Palm kernel at the origin. For a stationary DPP,

$$p_0 = \rho^{-1} \int |K_0(x)|^2 dx.$$

For our Gaussian-like DPP in Corollary 2.3, standard computations lead to $p_0 = \rho \pi^{d/2} c^{-1}$, which shows that the amount of repulsiveness in the process does not depend on Λ . Observe that is now evident the trade-off between intensity and repulsiveness: for a fixed p_0 , one cannot simultaneously increase the intensity ρ and $K_0(x)$ (for any fixed x). In particular, let us define the interaction range as $r_\varepsilon = \sup\{\|x\| : K_0(x) > \varepsilon\}$, which can be interpreted as the maximum distance at which two points influence each other, where ε is a threshold below which we assume that interaction is negligible. Then, for a fixed p_0 , large values of ρ correspond to small values of r_ε . That is, $K_0(x)$ decays faster as ρ increases.

2.3 The APPLAM model

The model we propose, called anisotropic repulsive point process latent mixture model, denoted APPLAM as mentioned before, assumes likelihood (2). We complete the prior specification as follows. We assume that $\{\mu_1, \dots, \mu_m\}$ is an anisotropic DPP conditioned on $m \geq 1$, i.e. it has a density with respect to a unit-rate Poisson point process on a compact $R \subset \mathbb{R}^d$ given by

$$\begin{aligned} p(\{\mu_1, \dots, \mu_m\} | \Lambda) &= f_{\text{DPP}}(\boldsymbol{\mu} | \rho, \Lambda, K_0; R) \\ &= \frac{e^{|R|-D}}{1 - e^{-D}} \det\{C(\mu_h, \mu_k)\}_{h,k=1,\dots,m}, \quad m \geq 1, \mu_1, \dots, \mu_m \in R \end{aligned} \quad (11)$$

and $p(\emptyset | \Lambda) = 0$, where D and C are defined just after (5). A possible choice of the compact set R is discussed in Section 4.2.

Conditional to $\{\mu_1, \dots, \mu_m\}$, indeed conditionally only to m , we assume

$$\begin{aligned} w_1, \dots, w_m | m &\sim \text{Dirichlet}(\alpha, \dots, \alpha) \\ \Delta_1, \dots, \Delta_m | m &\stackrel{\text{iid}}{\sim} \text{IW}_d(\nu_0, \Psi_0) \end{aligned} \quad (12)$$

where $\text{IW}_d(\nu_0, \Psi_0)$ denotes the d -dimensional inverse Wishart distribution, with $\nu_0 > d - 1$ degrees of freedom and mean $\Psi_0/(\nu_0 - d - 1)$. As in Chandra et al. (2020) we assume that the diagonal elements σ_j^2 of Σ , the covariance matrix of datapoints, are such that

$$\sigma_j^2 \stackrel{\text{iid}}{\sim} \text{inv-Gamma}(a_\sigma, b_\sigma), \quad j = 1, \dots, p, \quad (13)$$

i.e., their marginal prior distribution is inverse Gamma with mean $b_\sigma/(a_\sigma - 1)$. The Dirichlet-Laplace prior (Bhattacharya & Dunson, 2011) with parameter a is assumed as

the marginal prior for the matrix Λ , that is, denoting with λ_{jh} 's the elements of Λ ,

$$\begin{aligned} \lambda_{jh} \mid \phi, \tau, \psi &\stackrel{\text{ind}}{\sim} \mathcal{N}(0, \psi_{jh} \phi_{jh}^2 \tau^2), \quad j = 1, \dots, p; h = 1, \dots, d \\ \text{vec}(\phi) &\sim \text{Dirichlet}(a, \dots, a), \quad \psi_{jh} \stackrel{\text{iid}}{\sim} \text{Exp}(1/2), \quad \tau \sim \text{Gamma}(pda, 1/2) \end{aligned} \quad (14)$$

where, for any $p \times d$ matrix A , $\text{vec}(A)$ denotes the vector of dimension $p \times d$ such that $\text{vec}(A)_{p(h-1)+j} = (A)_{j,h}$. Note also that we have assumed prior independence among the blocks of parameters above.

3 Posterior Simulation

3.1 Approximation of the DPP density

The point process density in (11) cannot be evaluated in close form due to the infinite series in the expression of D and C . We follow Lavancier et al. (2015) and approximate it as follows. We first focus on $S = [-1/2, 1/2]^d$ and we set the point process density $f_{\text{DPP}}^{\text{app}}$, which is as in (11) where D and C are replaced by

$$D^{\text{app}} = - \sum_{k \in \mathbb{Z}_N^d} \log(1 - \varphi(k)), \quad C^{\text{app}}(x, y) = \sum_{k \in \mathbb{Z}_N^d} \frac{\varphi(k)}{1 - \varphi(k)} \exp(2\pi i \langle k, x - y \rangle) \quad (15)$$

where $\mathbb{Z}_N^d = \{-N, \dots, N\}^d$ and $\langle \cdot, \cdot \rangle$ denotes the scalar product. Note that $\boldsymbol{\mu} \sim f_{\text{DPP}}^{\text{app}}(\rho, \Lambda, C^{\text{app}}; S)$ is still a DPP on S , conditioned that it is nonempty. The truncation level N controls the goodness of the approximation of the density. Moreover, from (Equation (2.10) in Lavancier et al., 2015), the truncation level also sets an upper bound on the number of points in the DPP. Since the purpose of repulsive mixtures is to favour small values for the number of components, we found that small values of N , such as $N = 3, 5$, have no negative impact on posterior inference, but make the MCMC algorithm substantially faster.

To define the prior for the μ_h 's on a hyperrectangular region R different from $[-1/2, 1/2]^d$, it is sufficient to consider an affine transformation $T : R \rightarrow S$ and perform a change of variable leading to the following expression for $f_{\text{DPP}}^{\text{app}}(\boldsymbol{\mu} \mid \rho, \Lambda, C^{\text{app}}; R)$:

$$|R|^{-m} \frac{e^{|R| - D^{\text{app}}}}{1 - e^{-D^{\text{app}}}} \det\{C^{\text{app}}(T\mu_h, T\mu_k)\}_{h,k=1,\dots,m}, \quad m \geq 1, \mu_1, \dots, \mu_m \in R.$$

A specific strategy to fix R starting from the observations is described in Section 4.2.

3.2 The Gibbs sampling algorithm

Prior formulation as in the first line of (12) is not suitable for posterior inference as the sum-to-one constraint on \boldsymbol{w} leads to complex split-merge reversible jump moves with poor mixing of the chain. As in Beraha et al. (2022), we consider the following equivalent characterization of the prior for \boldsymbol{w}

$$\boldsymbol{w} = \left(\frac{S_1}{T}, \dots, \frac{S_m}{T} \right), \quad T = \sum_{h=1}^m S_h, \quad S_h \stackrel{\text{iid}}{\sim} \text{Gamma}(\alpha, 1). \quad (16)$$

Conditional to \mathbf{c} we consider $\boldsymbol{\mu} = \boldsymbol{\mu}^{(a)} \cup \boldsymbol{\mu}^{(na)}$, $\mathbf{S} = [\mathbf{S}^{(a)}, \mathbf{S}^{(na)}]$ and $\boldsymbol{\Delta} = [\boldsymbol{\Delta}^{(a)}, \boldsymbol{\Delta}^{(na)}]$, divided into allocated and non-allocated components, and denoted with the (a) and (na) superscripts, respectively. That is, $\boldsymbol{\mu}^{(a)} = \{\mu_{c_i}, i = 1, \dots, n\}$, $\boldsymbol{\mu}^{(na)} = \boldsymbol{\mu} \setminus \boldsymbol{\mu}^{(a)}$, and analogously for the terms involving the S_h 's and Δ_h 's.

Combining the likelihood (2) with the prior as in (11)-(14), we can see that the joint distribution of data and parameters has a density, with respect to some dominating measure on the proper space; see Appendix B for this density and the associated dominating measure. Normalization of the weights leads to a term $T^{-n} = (\sum S_{h_1}^{(a)} + \sum S_{h_2}^{(na)})^{-n}$ in the expression of the joint density, which makes it impossible to factorize the density according to the allocated and non-allocated components. To overcome this issue, as in Beraha et al. (2022), we introduce an auxiliary random variable $u | T \sim \text{Gamma}(n, T)$. We report the joint density of data and parameters in Appendix B.

We propose a Gibbs sampler algorithm, recurring to a Metropolis step when the corresponding full-conditionals cannot be sampled directly. Most of the updates are straightforward, except for two steps that are outlined below. The description of the algorithm is in Appendix D.

To update the non-allocated variables $(\boldsymbol{\mu}^{(na)}, \mathbf{s}^{(na)}, \boldsymbol{\Delta}^{(na)})$, we disintegrate the joint full-conditional of the non-allocated variables as

$$p(\boldsymbol{\mu}^{(na)}, \mathbf{s}^{(na)}, \boldsymbol{\Delta}^{(na)} | \text{rest}) = p(\boldsymbol{\mu}^{(na)} | \text{rest})p(\mathbf{s}^{(na)} | \boldsymbol{\mu}^{(na)}, \text{rest})p(\boldsymbol{\Delta}^{(na)} | \boldsymbol{\mu}^{(na)}, \text{rest}),$$

where ‘‘rest’’ identifies all the variables except for $(\boldsymbol{\mu}^{(na)}, \mathbf{s}^{(na)}, \boldsymbol{\Delta}^{(na)})$. Then $\boldsymbol{\mu}^{(na)} | \text{rest}$ is a Gibbs point process with density

$$p(\{\mu_1^{(na)}, \dots, \mu_\ell^{(na)}\} | \text{rest}) \propto f_{\text{DPP}}^{\text{app}}(\{\mu_1^{(na)}, \dots, \mu_\ell^{(na)}\} \cup \boldsymbol{\mu}^{(a)} | \rho, \Lambda, K_0; R)\psi(u)^\ell$$

where $\psi(u) = \mathbb{E}[e^{-uS}]$. See also Beraha et al. (2022). We employ the birth-death Metropolis-Hastings algorithm in Geyer & Møller (1994) to sample from this point process density. Given $\boldsymbol{\mu}^{(na)}$ it is straightforward to show

$$\begin{aligned} \Delta_1^{(na)}, \dots, \Delta_\ell^{(na)} &| \dots \stackrel{\text{iid}}{\sim} \text{IW}_d(\nu_0, \Psi_0) \\ S_1^{(na)}, \dots, S_\ell^{(na)} &| \dots \stackrel{\text{iid}}{\sim} \text{Gamma}(\alpha, 1 + u) \end{aligned}$$

To update of the latent allocation variables \mathbf{c} , we found it useful to marginalize over the η_i 's to get better mixing chains. Hence, we can sample each c_i independently from a discrete distribution over $\{1, \dots, k + \ell\}$, where k is the number of allocated components, with weights ω_{ih} :

$$\begin{aligned} \omega_{ih} &\propto S_h^{(a)} \mathcal{N}_p(y_i | \Lambda \mu_h^{(a)}, \Sigma + \Lambda \Delta_h^{(a)} \Lambda^\top), & h = 1, \dots, k \\ \omega_{ik+h} &\propto S_h^{(na)} \mathcal{N}_p(y_i | \Lambda \mu_h^{(na)}, \Sigma + \Lambda \Delta_h^{(na)} \Lambda^\top), & h = 1, \dots, \ell \end{aligned}$$

Each evaluation of the p -dimensional Gaussian density would require $\mathcal{O}(p^3)$ operations if care is not taken. However, we take advantage from the special structure of the covariance matrix. Using Woodbury's matrix identity, we have that

$$(\Sigma + \Lambda \Delta \Lambda^\top)^{-1} = \Sigma^{-1} - \Sigma^{-1} \Lambda (\Delta^{-1} + \Lambda^\top \Sigma^{-1} \Lambda)^{-1} \Lambda^\top \Sigma^{-1},$$

and hence we need now to compute the inverse of a $d \times d$ matrix. Therefore, evaluating the quadratic form in the exponential requires only $\mathcal{O}(p)$ computational cost. Moreover, using the matrix determinant lemma, the determinant of the covariance matrix can be computed as

$$\det(\Sigma + \Lambda\Delta\Lambda^\top) = \det(\Delta^{-1} + \Lambda^\top\Sigma^{-1}\Lambda) \det(\Delta) \det(\Sigma).$$

This is computed without additional cost by caching operations from the matrix inversion.

3.3 Updating Λ using gradient-based MCMC algorithms

As mentioned in Section 2.1, sampling from Λ 's full conditional is non-trivial. In particular, we found that random-walk Metropolis-Hastings led to very poor mixing of the MCMC chain, while the adaptive Metropolis-Hastings algorithm in Haario et al. (2001) is not feasible here due to the high dimensionality of Λ . Instead, we found the Metropolis adjusted Langevin Algorithm (MALA Roberts & Tweedie, 1996) to be more adequate here. The target density is

$$p(\Lambda \mid \dots) \propto p(\mathbf{y} \mid \Lambda, \boldsymbol{\eta}, \Sigma) p(\Lambda \mid \phi, \tau, \psi) |R|^{-n} \frac{e^{1-D^{\text{app}}}}{1 - e^{-D^{\text{app}}}} \det[C^{\text{app}}](T\mu_1, \dots, T\mu_n). \quad (17)$$

Although not explicitly stated, D^{app} and C^{app} both depend on Λ .

To sample from (17) using MALA, we must evaluate $\nabla \log(p(\Lambda \mid \dots))$. In a preliminary investigation, we tried using automatic differentiation (AD, Griewank et al., 1989) to get $\nabla \log(p(\Lambda \mid \dots))$, as it requires only the implementation of a function evaluating $\log(p(\Lambda \mid \dots))$. Unfortunately, we found that this strategy is viable only in trivial scenarios, i.e. up to $p = 50$ and $d = 3$ due to RAM memory requirements. See Figure 5 in Appendix D. Therefore, in the following theorem, we provide the analytical expression of $\nabla \log(p(\Lambda \mid \dots))$ when the associated DPP is Gaussian-like. See Appendix C for the Whittle-Matérn DPP case.

Theorem 3.1. *Under the Gaussian-like DPP prior, the gradient of the log-full conditional density of Λ equals*

$$\begin{aligned} \nabla \log p(\Lambda \mid \dots) &= \Sigma^{-1} \sum_{i=1}^n (y_i - \Lambda\eta_i)\eta_i^\top - \frac{1}{(\psi \odot \phi^2)\tau^2} \odot \Lambda + \\ &\quad + (2\pi^2 c^{-\frac{2}{d}}) \sum_{k \in \mathbb{Z}_N^d} g^{(k)} \frac{\varphi(k)}{(1 - \varphi(k))^2} \left[\frac{1 - \varphi(k)}{1 - e^{-D^{\text{app}}}} - v_k^\top (C^{\text{app}})^{-1} u_k \right] \end{aligned}$$

where $\varphi(k)$ is defined in (10), \odot denotes the elementwise (Hadamard) product,

$$g^{(k)} = 2|\Lambda^\top\Lambda|^{\frac{1}{d}}\Lambda(\Lambda^\top\Lambda)^{-1} \left[\frac{1}{d}k^\top(\Lambda^\top\Lambda)^{-1}k\mathbf{1}_d - k((\Lambda^\top\Lambda)^{-1}k)^\top \right],$$

u_k and v_k are m -dimensional column vectors for each $k \in \mathbb{Z}^d$ with entries

$$(u_k)_j = e^{2\pi i\langle k, T\mu_j \rangle}, \quad (v_k)_j = e^{-2\pi i\langle k, T\mu_j \rangle}, \quad j = 1, \dots, m$$

and $C^{\text{app}} := C^{\text{app}}(T\mu_1, \dots, T\mu_n)$.

Figure 5 in Appendix D reports a comparison of the memory requirements and the runtime execution using the AD gradients or our analytical expressions. In particular, using the AD gradients requires roughly 100x more memory, which makes a significant difference in practice since this is the bottleneck of our algorithm. The runtimes are 10x larger when using AD as well. The stepsize parameter of the MALA algorithm is tuned running short preliminary chains to get an acceptance rate around 20%. In particular, we found that values between 10^{-8} and 10^{-10} usually give a good mixing of the MCMC chain.

4 Simulation Studies

4.1 Synthetic data generation

We illustrate the comparison between the APPLAM model based on the Gaussian-like DPP (10) and the Lamb model of Chandra et al. (2020). This assumes likelihood (2) and a Dirichlet process mixture with total mass α_{DP} and a Normal-inverse Wishart as base measure. We consider two different sets of simulated data, referred to as simulation studies A and B. Both settings imply misspecification of the two models we assume for clustering. Let $t_p(q, \Sigma, \nu)$ denote the multivariate p -dimensional Student t distribution with location q , scale matrix Σ and degrees of freedom ν . In simulation study A we simulate 50 iid $\eta_i \in \mathbb{R}^d$ from each of $m = 4$ Gaussian kernels with means μ_h , $h = 1, \dots, m$, and identity covariance matrices. Then we simulate

$$y_i \mid \eta_i, \Lambda, \Sigma \stackrel{\text{ind}}{\sim} t_p(y_i \mid \Lambda \eta_i, \Sigma, 3) \quad i = 1, \dots, n$$

where $\Sigma = 0.5I_p$. See Appendix E for the values of the μ_h 's and Λ . For simulation B, the true latent factors are generated from each of $m = 4$ multivariate Student t distributions $t_d(\mu_h, I_d, 3)$, $h = 1, \dots, m$, with μ_h 's fixed as in simulation study A. Then $n = 200$ datapoints are independently generated from the likelihood in (2), with $\Sigma = 0.5I_p$ and Λ fixed as in simulation study A. For both simulation settings A and B, we consider $p = \{100, 200, 400\}$ and $d = \{2, 5, 8\}$. All the datapoints have been standardized before fitting the two models.

4.2 Hyperparameters elicitation and MCMC details

First, we discuss the choice of the hypersquare R where the DPP is supported, see (11). In Beraha et al. (2022), where p -dimensional data are directly modelled from the repulsive location mixture, R is fixed as the smallest hyperrectangle containing all the observations. Note that this procedure implicitly introduces anisotropy on the resulting point process if R is not a hypersquare. In a similar fashion, here we first estimate empirically the range of values for the η_i 's in (2) starting from the observations, and set R to be a hypersquare that covers this range of values. Specifically, we sample 100 draws from the prior distribution of Λ , denoted with $\tilde{\Lambda}_g$, $g = 1, \dots, 100$; then, we compute $\tilde{\eta}_{g,i}$, as the least-squares solution of $\tilde{\Lambda}_g \tilde{\eta}_{g,i} = y_i$; finally, we set $R = [-\gamma, \gamma]^d$ where $\gamma = 10 \max_{g,i} \|\tilde{\eta}_{g,i}\|_\infty$ and $\|\cdot\|_\infty$ is the

sup-norm. Numerical simulations show that posterior inference is robust with respect to the choice of R .

The elicitation for the common hyperparameters in APPLAM and Lamb follows the default choices of Chandra et al. (2020). See Appendix E for the numerical values of all hyperparameters. However, it is difficult to match the prior for the number of clusters in APPLAM and Lamb: while for Lamb it is determined by α_{DP} , for APPLAM it is induced by the prior for the number of components m , which is controlled by (ρ, c) . In particular, ρ is the prior expected number of components if we do not condition on $m \geq 1$. Therefore, we limit ourselves to evaluate empirically the robustness of the cluster estimates to the choice of these parameters in our simulations. In particular, we consider $\alpha_{DP} = \{0.1, 0.5, 1\}$, which corresponds to prior expected number of clusters of 1.57, 3.63, and 5.88, respectively. For our model instead, we set c_ρ such that $\rho = \rho_{max}/2$ as in Bianchini et al. (2020), and consider $\rho = \{5, 10, 20\}$.

For each run of the APPLAM model, we perform $2 \cdot 10^3$ burn-in iterations and $4 \cdot 10^3$ iterations with thinning equal to 5. For each run of the Lamb model instead, we perform 10^6 burn-in iterations and $5 \cdot 10^4$ iterations with thinning equal to 10. The poor mixing of the Lamb algorithm in our simulations (see Figure 6, Appendix D) demands a very long burn-in phase.

4.3 Comparison between the two models

Figures 2 and 3 show the posterior distribution of the number of clusters for our model and Lamb in the two simulation settings. Moreover, in the Appendix, we report posterior summary statistics of the random partition of the subjects in the sample induced by the allocation variables c_i 's such as the mode and mean of the number of clusters, the 95% credible interval for the adjusted rand index (ARI) between the random and true clustering. We also report the ARI between the estimated partition (obtained by minimizing posterior expectation of the Binder's loss function (Binder, 1978)) and the true one. See Tables 1 - 3 and Tables 4 - 6 for simulation studies A and B, respectively.

For both data generation processes, all the datasets we fit to the models, differing for the values of p and d , agree on the sensitivity of Lamb estimates to α_{DP} . In general, we see from the figures that Lamb tends to estimate a larger number of clusters than the truth ($m = 4$). On the other hand, APPLAM appears rather robust to the choice of ρ : not only is the estimated number of clusters always moderate (hardly more than 9), but most of the time the MCMC finds the correct number of clusters. Note the different scales for APPLAM and Lamb boxplots in Figures 2 and 3.

When looking at the ARI between the estimated partition and the true one, or at the credible intervals of the ARI of the random clustering, in case of scenario A, we see that for 24 out of 27 datasets, APPLAM provides better cluster estimates than Lamb. In particular, in several settings, the ARI between the estimated random partition and the true one for APPLAM is equal or close to 1.0 (i.e., perfect cluster detection) while for Lamb is smaller than 0.1 (i.e., almost random guessing). For scenario B instead, APPLAM provides better cluster estimates than Lamb 17 times out of 27 datasets.

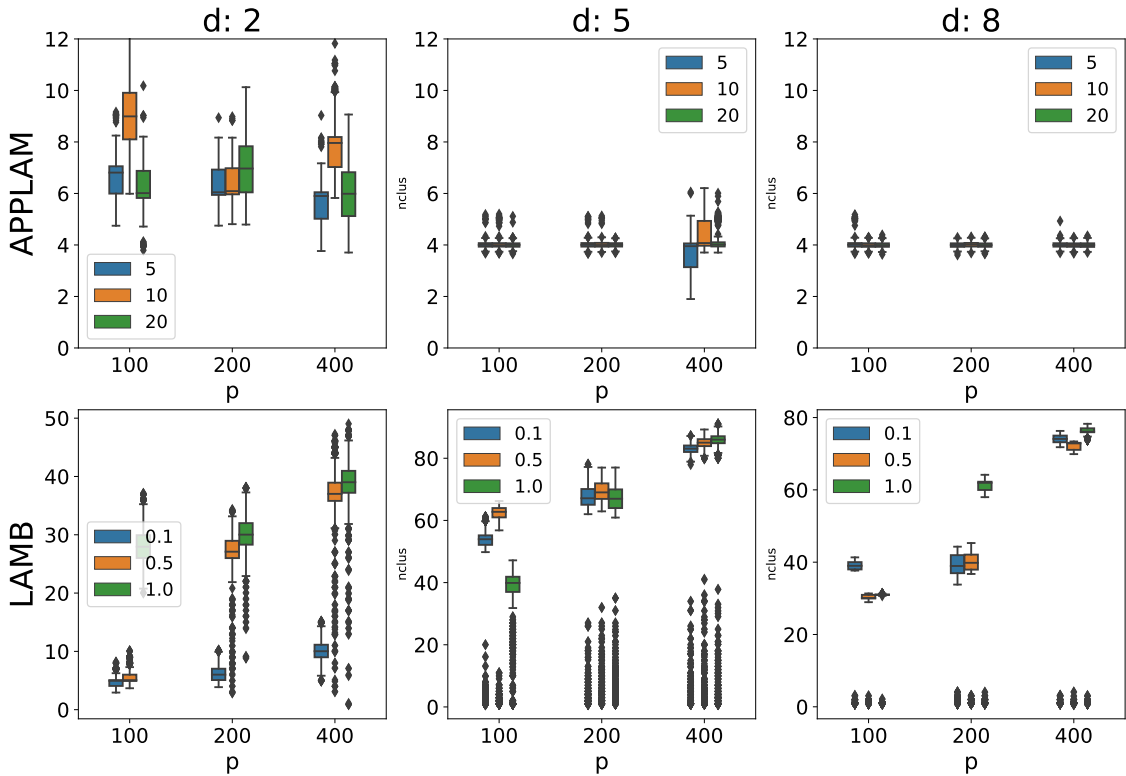


Figure 2: Boxplots of the posterior distribution of the number of clusters in simulation A, for APPLAM (top row) and Lamb (bottom row). Each panel corresponds to a different value of d as the dimension p and ρ or α_{DP} vary.

5 Joint Species Modeling

We apply our APPLAM model to data collecting the occurrence of plant species at different sites of the Bauges Natural Regional Park, in France. The data are available from the Alpine Botanical Conservatory (CBNA) and have been previously investigated by Bystrova et al. (2021) and Thuiller et al. (2018). Specifically, the dataset we analyze refers to $n = 1139$ sites and, for each site, the presence-absence of $p = 123$ different plant species is reported. Our goal is to infer the clustering structure of the sites, such that sites belonging to the same cluster show similar patterns concerning the occurrence of the plant species. Note that the data are binary; precisely, let $z_i \in \{0, 1\}^p$, $i = 1, \dots, n$, such that $z_{i,j} = 1$ if the plant species j occurs at the site i , $z_{i,j} = 0$ otherwise. We assume $z_{i,j} = \mathbb{1}_{[0,\infty)}(y_{i,j})$ and apply the APPLAM model to the y_i 's, assuming the Gaussian-like DPP. For identifiability reasons, we fix Σ in (2) as the $p \times p$ identity matrix and the Δ_h 's in (12) as the $d \times d$ identity matrix. Posterior simulation requires minor modifications to the Gibbs sampling algorithm, and we discuss them in Appendix D.

Prior parameters are chosen by model selection using the WAIC (Watanabe, 2013) index. Specifically, we consider $d \in \{3, 4\}$, $\alpha \in \{30, 50\}$ (see (16)), $\rho \in \{30, 40, 50\}$ and set the hypersquare $R = [-s/2, s/2]^d$ where $s \in \{30, 40, 50\}$, while fixing c such that $\rho = \rho_{\max}/2$ (see Corollary 2.3). The parameter a in (14) is fixed to 0.5 as suggested in

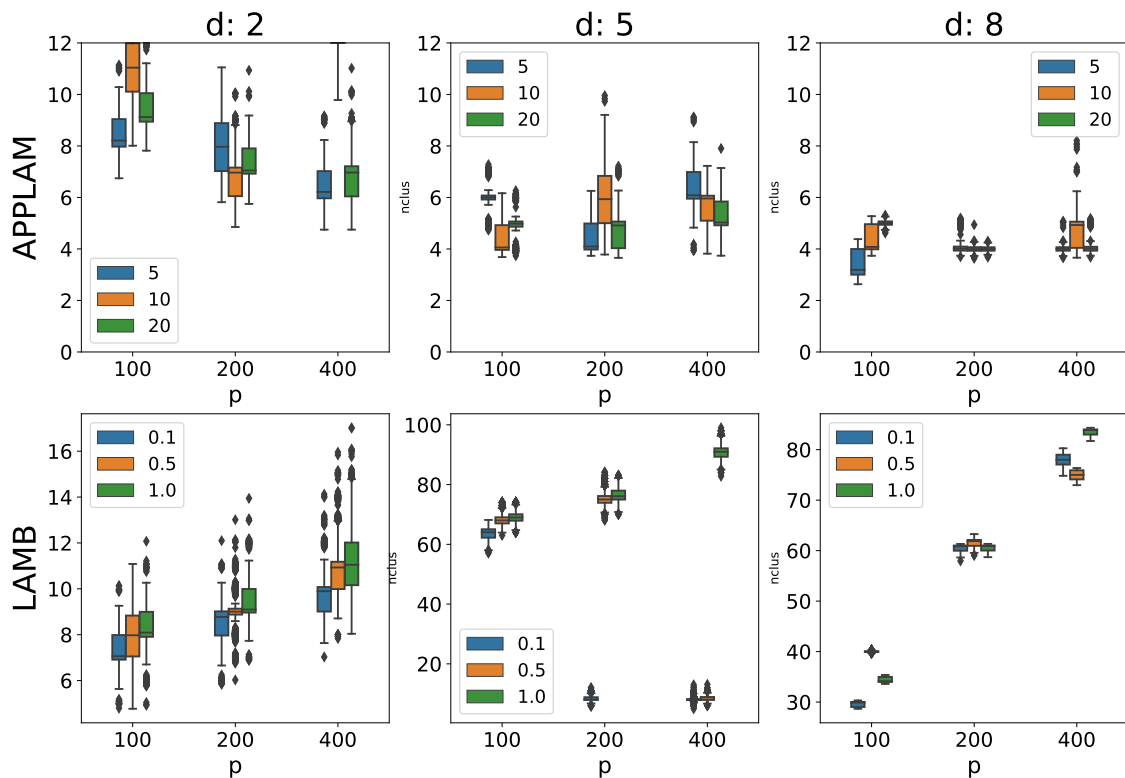


Figure 3: Boxplots of the posterior distribution of the number of clusters in simulation B, for APPLAM (top row) and Lamb (bottom row). Each panel corresponds to a different value of d as the dimension p and ρ or α_{DP} vary.

Chandra et al. (2020). We fit the 36 models separately by running the MCMC algorithm for 10^4 burn-in iterations and $4 \cdot 10^3$ iterations with thinning equal to 5. The best model (the largest WAIC) corresponds to dimension $d = 4$, with $\alpha = 30$, $\rho = 50$, $s = 50$, although all models showed similar WAIC values. We obtain a point estimate of the clusters by minimizing the posterior expectation of the Binder's loss function. According to this estimate, the model identifies $C = 5$ well-balanced clusters of sites in the sample. To interpret the estimated clusters, we look at the patterns of presence/absence of species in each cluster. Specifically, for $j = 1, \dots, p$, let \bar{z}_j and $\bar{z}_{c,j}$ be the empirical frequency of the j -th species in the whole sample and in the c -th cluster, respectively. For each cluster, we select six species that better represent it by choosing the three species that maximize (resp. minimize) $\delta_{c,j} = (\bar{z}_{c,j} - \bar{z}_j)$. In total, we find 23 species that best describe the different clusters. We report the corresponding $\delta_{c,j}$'s in Figure 4. We notice that cluster 2 is mainly characterized by absences, i.e. the $\delta_{2,j}$'s are mostly negative. Cluster 3 stands out for the large presence of species 22, 72, and 77. Cluster 4 has in general large values of $\delta_{4,j}$'s, both negative and positive. We also report the posterior estimate of $\Lambda\Lambda^\top$ restricted on the 23 species found above in Figure 4.

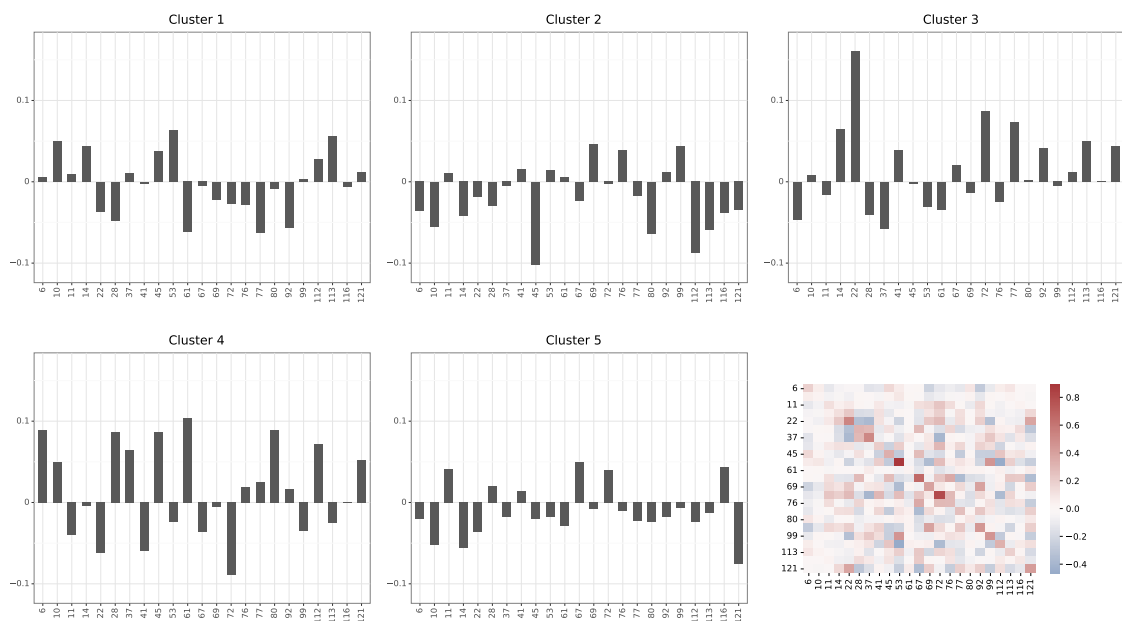


Figure 4: Values of $\delta_{c,j}$ for the 23 species identifying the five clusters and (bottom right) posterior estimate of $\Lambda\Lambda^\top$ restricted on the 23 species. The species labels are associated as follows. “6”: *Hedera helix* L. - “10”: *Hieracium murorum* L. - “11”: *Homogyne alpina* (L.) Cass. - “14”: *Prenanthes purpurea* L. - “22”: *Phyteuma spicatum* L. - “28”: *Corylus avellana* L. - “37”: *Mercurialis perennis* L. - “41”: *Lotus corniculatus* L. - “45”: *Fagus sylvatica* L. - “53”: *Lamium galeobdolon* (L.) L. subsp. *montanum* (Pers.) Hayek - “61”: *Fraxinus excelsior* L. - “67”: *Rumex arifolius* All. - “69”: *Lysimachia vulgaris* L. - “72”: *Ranunculus tuberosus* Lapeyr. - “76”: *Filipendula ulmaria* (L.) Maxim. - “77”: *Fragaria vesca* L. - “80”: *Sorbus aria* (L.) Crantz - “92”: *Carex sylvatica* Hudson - “99”: *Briza media* L. - “112”: *Abies alba* Miller - “113”: *Picea abies* (L.) Karsten - “116”: *Carduus defloratus* L. subsp. *defloratus* - “121”: *Rubus fruticosus* groupe.

6 Discussion

Model-based clustering of moderate or large dimensional data is notoriously difficult. We have proposed a model for simultaneous dimensionality reduction and clustering, by assuming a mixture model for the latent scores, which are then linked to the observations via a Gaussian latent factor model. This approach was recently investigated by Chandra et al. (2020). The authors use a factor-analytic representation and assume a mixture model for the latent factors. However, performance can deteriorate in the presence of model misspecification. Assuming a repulsive point process prior for the component-specific means of the mixture for the latent scores is shown to yield a more robust model that outperforms the standard Lamb on several simulated scenarios. To favor well-separated clusters of data, the repulsive point process must be anisotropic, and its density should be tractable for efficient posterior inference. We address these issues by proposing a general construction for anisotropic determinantal point processes.

The bottleneck in our simulation algorithm is the spectral approximation of the den-

sity of the DPP that has a computational cost that scales exponentially in d , the dimension of the latent factors. It is common practice to set small values for d in latent factor models. Nonetheless, for moderate or large values of d the approach in Bardenet & Titsias (2015) would be more efficient, at the price that the parameters in the model are harder to interpret. Another approximation of the DPP density is provided by Poinas & Lavancier (2021), suitable also for non (hyper-)rectangular domains. In the case of projection DPPs, i.e. when the eigenvalues of the spectral decomposition are either zero or one, we could sample exactly from the full-conditional of the non-allocated components using the methods in Lavancier & Rubak (2023) instead of employing a birth-death Metropolis-Hastings move.

We have not investigated the estimation of the factor loading matrix Λ , which could be of interest to explain the correlation structure of the data. Our model inherits the rotational invariance property of classical factor models, but this issue can be dealt with via *ex post* procedures for the estimation of Λ . See, for instance, Papastamoulis & Ntzoufras (2022) and the references therein.

References

- ASCOLANI, F., LIJOI, A., REBAUDO, G. & ZANELLA, G. (2022). Clustering consistency with Dirichlet process mixtures. *Biometrika* .
- BACCELLI, F., BŁASZCZYŚYŃ, B. & KARRAY, M. (2020). Random measures, point processes, and stochastic geometry. *HAL preprint available at <https://hal.inria.fr/hal-02460214/>* .
- BARDENET, R. & TITSIAS, M. (2015). Inference for determinantal point processes without spectral knowledge. In *Advances in Neural Information Processing Systems*, C. Cortes, N. Lawrence, D. Lee, M. Sugiyama & R. Garnett, eds., vol. 28. Curran Associates, Inc.
- BERAHA, M., ARGIENTO, R., MØLLER, J. & GUGLIELMI, A. (2022). MCMC computations for Bayesian mixture models using repulsive point processes. *J. Comp. Graph. Stat.* , 1–14.
- BHATTACHARYA, A. & DUNSON, D. B. (2011). Sparse bayesian infinite factor models. *Biometrika* , 291–306.
- BHATTACHARYA, A., PATI, D., PILLAI, N. S. & DUNSON, D. B. (2015). Dirichlet–laplace priors for optimal shrinkage. *J. Am. Stat. Assoc.* **110**, 1479–1490.
- BIANCHINI, I., GUGLIELMI, A. & QUINTANA, F. A. (2020). Determinantal point process mixtures via spectral density approach. *Bayes. Anal.* **15**, 187–214.
- BINDER, D. A. (1978). Bayesian cluster analysis. *Biometrika* **65**, 31–38.
- BISCIO, C. A. N. & LAVANCIER, F. (2016). Quantifying repulsiveness of determinantal point processes. *Bernoulli* **22**, 2001–2028.

- BYSTROVA, D., POGGIATO, G., BEKTAŞ, B. & ARBEL, E. A. (2021). Clustering species with residual covariance matrix in joint species distribution models. *Frontiers in Ecology and Evolution* **9**.
- CAI, D., CAMPBELL, T. & BRODERICK, T. (2021). Finite mixture models do not reliably learn the number of components. In *International Conference on Machine Learning*. PMLR.
- CELEUX, G., KAMARY, K., MALSINER-WALLI, G., MARIN, J.-M. & ROBERT, C. P. (2019). Computational solutions for bayesian inference in mixture models. *Handbook of Mixture Analysis* , 73–96.
- CHANDRA, N. K., CANALE, A. & DUNSON, D. B. (2020). Escaping the curse of dimensionality in bayesian model based clustering. *arXiv preprint arXiv:2006.02700* .
- DALEY, D. J. & VERE-JONES, D. (2008). *An introduction to the theory of point processes. Vol. II. Probability and its Applications* (New York). New York: Springer, 2nd ed. General theory and structure.
- DUAN, L. L. & DUNSON, D. B. (2021). Bayesian distance clustering. *J. Mach. Learn. Res.* **22**, 1–27.
- FRUHWIRTH-SCHNATTER, S., CELEUX, G. & ROBERT, C. P. (2019). *Handbook of mixture analysis*. CRC press.
- GEYER, C. J. & MØLLER, J. (1994). Simulation procedures and likelihood inference for spatial point processes. *Scandinavian Journal of Statistics* **21**, 359–373.
- GRIEWANK, A. et al. (1989). On automatic differentiation. *Mathematical Programming: recent developments and applications* **6**, 83–107.
- HAARIO, H., SAKSMAN, E. & TAMMINEN, J. (2001). An adaptive Metropolis algorithm. *Bernoulli* **7**, 223 – 242.
- LAVANCIER, F., MØLLER, J. & RUBAK, E. (2015). Determinantal point process models and statistical inference. *J. R. Stat. Soc. Ser. B* **77**, 853–877.
- LAVANCIER, F. & RUBAK, E. (2023). On simulation of continuous determinantal point processes. *arXiv preprint arXiv:2301.11081* .
- LOPES, H. F. (2014). Modern bayesian factor analysis. *Bayesian Inference in the Social Sciences* , 115–153.
- MACCHI, O. (1975). The coincidence approach to stochastic point processes. *Adv. App. Prob.* **7**, 83–122.
- MALSINER-WALLI, G., FRUHWIRTH-SCHNATTER, S. & GRÜN, B. (2016). Model-based clustering based on sparse finite gaussian mixtures. *Stat. Comp.* **26**, 303–324.

- MILLER, J. W. & HARRISON, M. T. (2014). Inconsistency of pitman-yor process mixtures for the number of components. *J. Mach. Learn. Res.* **15**, 3333–3370.
- MØLLER, J. & O'REILLY, E. (2021). Couplings for determinantal point processes and their reduced palm distributions with a view to quantifying repulsiveness. *J. App. Prob.* **58**, 469–483.
- MØLLER, J., PETTITT, A. N., REEVES, R. & BERTHELSEN, K. K. (2006). An efficient markov chain monte carlo method for distributions with intractable normalising constants. *Biometrika* **93**, 451–458.
- MØLLER, J. & WAAGEPETERSEN, R. P. (2003). *Statistical inference and simulation for spatial point processes*. CRC Press.
- MURRAY, I., GHAHRAMANI, Z. & MACKAY, D. J. C. (2006). Mcmc for doubly-intractable distributions. In *Proceedings of the 22nd Conference on Uncertainty in Artificial Intelligence*. Arlington, Virginia, USA.
- NATARAJAN, A., DE IORIO, M., HEINECKE, A., MAYER, E. & GLENN, S. (2021). Cohesion and repulsion in bayesian distance clustering. *arXiv preprint arXiv:2107.05414* .
- NEAL, R. M. (2003). Density modeling and clustering using dirichlet diffusion trees.
- PAPASTAMOULIS, P. & NTZOUFRAS, I. (2022). On the identifiability of bayesian factor analytic models. *Statistics and Computing* **32**, 23.
- PETERSEN, K. B. & PEDERSEN, M. S. (2008). The matrix cookbook. Version 20081110.
- POINAS, A. & LAVANCIER, F. (2021). Asymptotic approximation of the likelihood of stationary determinantal point processes. *Scandinavian Journal of Statistics* .
- QUINLAN, J. J., QUINTANA, F. A. & PAGE, G. L. (2020). Parsimonious hierarchical modeling using repulsive distributions. *Test* (to appear) .
- ROBERTS, G. O. & TWEEDIE, R. L. (1996). Exponential convergence of langevin distributions and their discrete approximations. *Bernoulli* , 341–363.
- TEH, Y., DAUME III, H. & ROY, D. M. (2007). Bayesian agglomerative clustering with coalescents. *NeurIPS* **20**.
- THUILLER, W., GUÉGUEN, M., BISON, M. & DUPARC, E. A. (2018). Combining point-process and landscape vegetation models to predict large herbivore distributions in space and time—a case study of rupicapra rupicapra. *Diversity and Distributions* **24**, 352–362.
- WATANABE, S. (2013). A widely applicable bayesian information criterion. *J. Mach. Learn. Res.* **14**, 867–897.

XIE, F. & XU, Y. (2019). Bayesian repulsive gaussian mixture model. *J. Am. Stat. Assoc.*, 187–203.

A Proofs

A.1 Proof of Theorem 2.1

Proof. Since Λ is full rank, $\Lambda^T \Lambda$ is positive definite and invertible, so that the conditional distribution (6) for Y is well-defined. Denoting with $|\Lambda^T \Lambda|$ the determinant of $\Lambda^T \Lambda$, we explicitly compute the marginal density $h(x)$ of Y . We have:

$$h(x) = \int_0^{+\infty} p(x|w) \cdot p(w) dw = \int_0^{+\infty} \frac{|\Lambda^T \Lambda|^{\frac{1}{2}}}{(2\pi)^{\frac{d}{2}} w^{\frac{d}{2}}} \exp\left(-\frac{x^T \Lambda^T \Lambda x}{2w}\right) \cdot p(w) dw$$

Therefore, we derive

$$h(x) = \frac{|\Lambda^T \Lambda|^{\frac{1}{2}}}{(2\pi)^{\frac{d}{2}}} \mathbb{E}\left[W^{-\frac{d}{2}} \exp\left(-\frac{|\Lambda x|^2}{2W}\right)\right], \quad x \in \mathbb{R}^d \quad (18)$$

Consequently, since $K_0(x) = \rho h(x)/h(0)$, we have

$$K_0(x) = \frac{\rho}{\mathbb{E}[W^{-\frac{d}{2}}]} \mathbb{E}\left[W^{-\frac{d}{2}} \exp\left(-\frac{|\Lambda x|^2}{2W}\right)\right], \quad x \in \mathbb{R}^d$$

and, since $\varphi = \mathcal{F}(K_0)$, we compute

$$\begin{aligned} \varphi(x) &= \int_{\mathbb{R}^d} e^{-2\pi i x^T y} K_0(y) dy = \\ &= \frac{\rho}{h(0)} \int_{\mathbb{R}^d} e^{-2\pi i x^T y} \frac{|\Lambda^T \Lambda|^{\frac{1}{2}}}{(2\pi)^{\frac{d}{2}}} \mathbb{E}\left[W^{-\frac{d}{2}} \exp\left(-\frac{|\Lambda y|^2}{2W}\right)\right] dy = \\ &= \frac{\rho |\Lambda^T \Lambda|^{\frac{1}{2}}}{h(0) (2\pi)^{\frac{d}{2}}} \int_{\mathbb{R}^d} e^{-2\pi i x^T y} \int_0^{\infty} w^{-\frac{d}{2}} \exp\left(-\frac{|\Lambda y|^2}{2w}\right) p(w) dw dy = \\ &= \frac{\rho |\Lambda^T \Lambda|^{\frac{1}{2}}}{h(0) (2\pi)^{\frac{d}{2}}} \int_0^{\infty} \int_{\mathbb{R}^d} w^{-\frac{d}{2}} \exp\left(-2\pi i x^T y - \frac{y^T \Lambda^T \Lambda y}{2w}\right) dy p(w) dw = \\ &= \frac{\rho |\Lambda^T \Lambda|^{\frac{1}{2}}}{h(0) (2\pi)^{\frac{d}{2}}} \int_0^{\infty} \int_{\mathbb{R}^d} w^{-\frac{d}{2}} \exp\left(-\frac{1}{2} \left[y^T \frac{\Lambda^T \Lambda}{w} y + 4\pi i x^T y \right]\right) dy p(w) dw \end{aligned}$$

The term in the squared brackets above can be written as

$$\begin{aligned} [\dots] &= (y - (-2\pi i w (\Lambda^T \Lambda)^{-1} x))^T \frac{\Lambda^T \Lambda}{w} (y - (-2\pi i w (\Lambda^T \Lambda)^{-1} x)) \\ &\quad + 4\pi^2 x^T w (\Lambda^T \Lambda)^{-1} x. \end{aligned}$$

If we plug it in in the last expression of $\varphi(x)$ we have:

$$\varphi(x) = \frac{\rho}{h(0)} \int_0^{+\infty} \exp(-2\pi^2 w x^T (\Lambda^T \Lambda)^{-1} x) p(w) dw .$$

Summing up, we derive

$$\varphi(x) = \frac{\rho}{h(0)} \mathbb{E} \left[\exp(-2\pi^2 W x^T (\Lambda^T \Lambda)^{-1} x) \right], \quad x \in \mathbb{R}^d .$$

Observe that, since $h(x)$ is the density of a real-valued random variable, using Fourier transform properties, then

$$K_0(x) = \rho \frac{h(x)}{h(0)} \in L^1(\mathbb{R}^d), \quad \varphi = \mathcal{F}(K_0) \in L^1(\mathbb{R}^d) .$$

Therefore, to guarantee the existence of the anisotropic determinantal point process with kernel K_0 and spectral density $\varphi = \mathcal{F}(K_0)$, we refer to Corollary (3.3) of Lavancier et al. (2015): since $K_0 \in L^1(\mathbb{R}^d)$, $\varphi = \mathcal{F}(K_0)$ and $\varphi \in L^1(\mathbb{R}^d)$, we just need to ensure

$$\varphi(x) \leq 1, \quad \forall x \in \mathbb{R}^d .$$

So, we need to assume

$$\max_{x \in \mathbb{R}^d} \varphi(x) = \varphi(0) = \frac{\rho}{h(0)} \leq 1 .$$

This assumption is equivalent to

$$\rho \leq \rho_{max}$$

where

$$\rho_{max} = h(0) = \frac{|\Lambda^T \Lambda|^{\frac{1}{2}}}{(2\pi)^{\frac{d}{2}}} \mathbb{E} \left[W^{-\frac{d}{2}} \right]$$

□

A.2 Proof of Theorem 2.2

Let $B := \Lambda \mathbb{R}^d$. Then $\Lambda : \mathbb{R}^d \rightarrow B$ is a bijective map. We perform a change of coordinates on B using the orthonormal basis given by the singular value decomposition of $\Lambda = U \Omega V^T$ where U is a $p \times d$ matrix whose columns are an orthonormal basis of B , Ω is a $d \times d$ diagonal matrix and V is a $d \times d$ orthogonal matrix. Let $\Lambda^* := \Omega V^T$ which maps \mathbb{R}^d into B expressed with the coordinates given by U .

Consider now the transformed points $\tilde{\mu}_h = \Lambda \mu_h$. These are clearly in a one-to-one relation with the points $\mu_h^* = \Lambda^* \mu_h$, given by $\tilde{\mu}_h = U \mu_h^*$. Then, it is sufficient to show that $\Phi^* = \{\mu_1^*, \dots, \mu_m^*\}$ is an isotropic DPP on $B^* = \Lambda^* \mathbb{R}^d = \mathbb{R}^d$. Consider a measurable function $h : B^{*k} \rightarrow \mathbb{R}_+$,

$$\mathbb{E} \sum_{\mathbf{y}_k^* \in \Phi^*}^{\neq} h(y_1^*, \dots, y_k^*) = \mathbb{E} \sum_{\mathbf{x}_k \in \Phi}^{\neq} h(\Lambda^* x_1, \dots, \Lambda^* x_k),$$

where the summation is intended over all k -tuples of pairwise disjoint points in the support of the point process. By the definition of the DPP

$$\begin{aligned}\mathbb{E} \sum_{\mathbf{y}_k^* \in \Phi^*}^{\neq} h(\mathbf{y}_1^*, \dots, \mathbf{y}_k^*) &= \mathbb{E} \sum_{\mathbf{x}_k \in \Phi}^{\neq} h(\Lambda^* x_1, \dots, \Lambda^* x_k) \\ &= \int_{(\mathbb{R}^d)^k} \det\{K(x_i, x_j)\}_{i,j=1,\dots,k} h(\Lambda^* x_1, \dots, \Lambda^* x_k) dx_1 \cdots dx_k \\ &= \int_{B^{*k}} \det\{K((\Lambda^*)^{-1} y_i^*, (\Lambda^*)^{-1} y_j^*)\}_{i,j=1,\dots,k} h(\mathbf{y}_1^*, \dots, \mathbf{y}_k^*) \det(\Lambda^*)^{-k} dy_1^* \cdots dy_k^*\end{aligned}$$

which shows that $\Lambda^* \mu$ is a DPP on B^* with kernel given by $\det(\Lambda^*)^{-1} K((\Lambda^*)^{-1} y_i^*, (\Lambda^*)^{-1} y_j^*)$ and the dominating measure on B^* is the Lebesgue measure. Stationarity and isotropy follow by choosing $K \equiv K_0$ as in Theorem 2.1. Indeed,

$$\begin{aligned}K((\Lambda^*)^{-1} y_i^*, (\Lambda^*)^{-1} y_j^*) &= K_0((\Lambda^*)^{-1} (y_i^* - y_j^*)) \\ &= \frac{\rho}{W^{-d/2}} \mathbb{E} \left[W^{-d/2} e^{-\|y_i^* - y_j^*\|^2 / 2} \right]\end{aligned}$$

The result follows by noting that U is orthogonal (i.e., the map between the $\tilde{\mu}_j$ and μ_j^* is an isometric bijection) and that $\det(\Lambda^*) = \det(\Lambda^\top \Lambda)^{1/2}$.

A.3 Proof of Corollary 2.3

Proof. Let $c > 0$. In Theorem 2.1, set

$$W = |\Lambda^\top \Lambda|^{\frac{1}{d}} \cdot c^{-\frac{2}{d}}$$

Consequently, $W^{-\frac{d}{2}} = |\Lambda^\top \Lambda|^{-\frac{1}{2}} \cdot c$, and from Equation (18), we derive

$$h(x) = \frac{c}{(2\pi)^{\frac{d}{2}}} \cdot \exp\left(-\frac{\|\Lambda x\|^2}{2|\Lambda^\top \Lambda|^{\frac{1}{d}} c^{-\frac{2}{d}}}\right), \quad x \in \mathbb{R}^d.$$

From Equations (8) and (9), we have

$$\begin{aligned}K_0(x) &= \rho \cdot \exp\left(-\frac{\|\Lambda x\|^2}{2|\Lambda^\top \Lambda|^{\frac{1}{d}} c^{-\frac{2}{d}}}\right), \quad x \in \mathbb{R}^d \\ \varphi(x) &= \rho \frac{(2\pi)^{\frac{d}{2}}}{c} \cdot \exp\left(-2\pi^2 |\Lambda^\top \Lambda|^{\frac{1}{d}} c^{-\frac{2}{d}} x^\top (\Lambda^\top \Lambda)^{-1} x\right), \quad x \in \mathbb{R}^d.\end{aligned}$$

From (7), the existence condition requires $\rho \leq \rho_{max}$, with

$$\rho_{max} = \frac{c}{(2\pi)^{d/2}}.$$

□

A.4 Proof of Theorem 3.1

Proof. Consider

$$\log p(\Lambda | \dots) \propto \log p(\mathbf{y} | \Lambda, \boldsymbol{\eta}, \Sigma) + \log f_{\text{DPP}}^{\text{app}}(\boldsymbol{\mu} | \Lambda) + \log p(\Lambda | \phi, \tau, \psi) \quad (19)$$

We compute the gradient of log-full conditional density of Λ summing up the gradients of the three terms above. Note that the only term depending on the anisotropic DPP is the second one. Since it is the most complex term, we derive it using the two lemmas below. For the first term of (19), we have

$$\begin{aligned} \nabla \log p(\mathbf{y} | \Lambda, \boldsymbol{\eta}, \Sigma) &= \nabla \left(-\frac{1}{2} \sum_{i=1}^n (y_i - \Lambda \eta_i)^\top \Sigma^{-1} (y_i - \Lambda \eta_i) \right) \\ &= \Sigma^{-1} \cdot \sum_{i=1}^n (y_i - \Lambda \eta_i) \eta_i^\top. \end{aligned}$$

The gradient of the last term is

$$\nabla \log p(\Lambda | \phi, \tau, \psi) = -\frac{1}{(\psi \odot \phi^2) \tau^2} \odot \Lambda.$$

The gradient of the second term of (19) is,

$$\begin{aligned} \nabla \log f_{\text{DPP}}^{\text{app}}(\boldsymbol{\mu} | \Lambda) &= \nabla [-D^{\text{app}} - \log(1 - e^{-D^{\text{app}}}) + \log \det[C^{\text{app}}](T\mu_1, \dots, T\mu_n)] \\ &= -\nabla D^{\text{app}} - \nabla \log(1 - e^{-D^{\text{app}}}) + \nabla \log \det[C^{\text{app}}](T\mu_1, \dots, T\mu_n) \\ &= -\frac{1}{1 - e^{-D^{\text{app}}}} \nabla D^{\text{app}} + \nabla \log \det[C^{\text{app}}](T\mu_1, \dots, T\mu_n) \quad (20) \end{aligned}$$

To handle (20), the terms ∇D^{app} and $\nabla \log \det[C^{\text{app}}](T\mu_1, \dots, T\mu_n)$ are to be computed.

Lemma A.1. *For the Gaussian-like DPP prior,*

$$\nabla D^{\text{app}} = \sum_{k \in \mathbb{Z}_N^d} \frac{\varphi(k)}{1 - \varphi(k)} (-2\pi^2 c^{-\frac{2}{d}}) g^{(k)} \quad (21)$$

where $\varphi(k)$ refers to (10).

Proof. Write

$$\nabla D^{\text{app}} = - \sum_{k \in \mathbb{Z}_N^d} \nabla \log(1 - \varphi(k)) = \sum_{k \in \mathbb{Z}_N^d} \frac{1}{1 - \varphi(k)} \nabla \varphi(k).$$

For the Gaussian-like DPP prior, from (10), observe that, for $k \in \mathbb{Z}^d$

$$\begin{aligned} \nabla \varphi(k) &= \frac{\rho}{c} (2\pi)^{\frac{d}{2}} \nabla \exp \left(-2\pi^2 |\Lambda^T \Lambda|^{\frac{1}{d}} c^{-\frac{2}{d}} k^T (\Lambda^T \Lambda)^{-1} k \right) \\ &= \varphi(k) \left(-2\pi^2 c^{-\frac{2}{d}} \right) \nabla \left(|\Lambda^T \Lambda|^{\frac{1}{d}} k^T (\Lambda^T \Lambda)^{-1} k \right). \end{aligned}$$

Note that

$$\begin{aligned}
\nabla \left(|\Lambda^T \Lambda|^{\frac{1}{d}} k^T (\Lambda^T \Lambda)^{-1} k \right) &= \nabla \left(|\Lambda^T \Lambda|^{\frac{1}{d}} \right) k^T (\Lambda^T \Lambda)^{-1} k + \\
&\quad + |\Lambda^T \Lambda|^{\frac{1}{d}} \nabla \left(k^T (\Lambda^T \Lambda)^{-1} k \right) = \\
&= \frac{1}{d} |\Lambda^T \Lambda|^{\frac{1}{d}-1} 2 |\Lambda^T \Lambda| \Lambda (\Lambda^T \Lambda)^{-1} k^T (\Lambda^T \Lambda)^{-1} k + \\
&\quad + |\Lambda^T \Lambda|^{\frac{1}{d}} \nabla \left(k^T (\Lambda^T \Lambda)^{-1} k \right)
\end{aligned}$$

where, in the last step, formula (53) of Petersen & Pedersen (2008) is used. Then,

$$\begin{aligned}
\nabla \left(k^T (\Lambda^T \Lambda)^{-1} k \right) &= \nabla \text{tr} \left(k^T (\Lambda^T \Lambda)^{-1} k \right) = \\
&= \nabla \text{tr} \left((\Lambda^T \Lambda)^{-1} k k^T \right) = -\Lambda (\Lambda^T \Lambda)^{-1} (2 k k^T) (\Lambda^T \Lambda)^{-1}
\end{aligned}$$

where, in the last step, we have applied formula (125) of Petersen & Pedersen (2008). For the Gaussian-like DPP prior, this leads to

$$\nabla \varphi(k) = \varphi(k) (-4\pi^2 c^{-\frac{2}{d}}) |\Lambda^T \Lambda|^{\frac{1}{d}} \Lambda (\Lambda^T \Lambda)^{-1} \left[\frac{1}{d} k^T (\Lambda^T \Lambda)^{-1} k \mathbb{1}_d - k k^T (\Lambda^T \Lambda)^{-1} \right] \quad (22)$$

where $\mathbb{1}_d$ is $d \times d$ matrix of 1's. This concludes the proof of Lemma A.1. \square

Lemma A.2. *For the Gaussian-like DPP prior,*

$$\nabla \log \det[C^{\text{app}}] = (-2\pi^2 c^{-\frac{2}{d}}) \sum_{k \in \mathbb{Z}_N^d} \frac{\varphi(k)}{(1 - \varphi(k))^2} g^{(k)} v_k^T (C^{\text{app}})^{-1} u_k \quad (23)$$

where $\varphi(k)$ refers to (10).

Proof. We have

$$\frac{\partial}{\partial \Lambda_{ij}} \log \det[C^{\text{app}}] = \text{tr} \left(\left(\frac{\partial}{\partial U} \log \det U \right) \Big|_{U=C^{\text{app}}} \cdot \frac{\partial}{\partial \Lambda_{ij}} C^{\text{app}} \right) \quad (24)$$

$$\begin{aligned}
&= \text{tr} \left(\frac{1}{\det[C^{\text{app}}]} \left(\frac{\partial}{\partial U} \det U \right) \Big|_{U=C^{\text{app}}} \cdot \frac{\partial}{\partial \Lambda_{ij}} C^{\text{app}} \right) \\
&= \text{tr} \left((C^{\text{app}})^{-1} \cdot \frac{\partial}{\partial \Lambda_{ij}} C^{\text{app}} \right) \quad (25)
\end{aligned}$$

where formula (137) of Petersen & Pedersen (2008) is used to get Equation (24) and formula (49) of Petersen & Pedersen (2008) for Equation (25). Now, note that

$$C^{\text{app}} = \sum_{k \in \mathbb{Z}_N^d} \frac{\varphi(k)}{1 - \varphi(k)} u_k v_k^T \quad (26)$$

where u_k, v_k are defined in the statement. It follows that, for the Gaussian-like DPP prior,

$$\frac{\partial}{\partial \Lambda_{ij}} C^{\text{app}} = \sum_{k \in \mathbb{Z}_N^d} \frac{\varphi(k)}{(1 - \varphi(k))^2} (-2\pi^2 c^{-\frac{2}{d}}) g_{ij}^{(k)} u_k v_k^T$$

where $g_{ij}^{(k)} = (g^{(k)})_{ij}$. Then, back to Equation (25), for the Gaussian-like DPP prior, we have

$$\begin{aligned}
\frac{\partial}{\partial \Lambda_{ij}} \log \det[C^{\text{app}}] &= \text{tr} \left((C^{\text{app}})^{-1} \cdot \frac{\partial}{\partial \Lambda_{ij}} C^{\text{app}} \right) \\
&= \text{tr} \left(\sum_{k \in \mathbb{Z}_N^d} \frac{\varphi(k)}{(1 - \varphi(k))^2} (-2\pi^2 c^{-\frac{2}{d}}) g_{ij}^{(k)} (C^{\text{app}})^{-1} u_k v_k^T \right) \\
&= \sum_{k \in \mathbb{Z}_N^d} \frac{\varphi(k)}{(1 - \varphi(k))^2} (-2\pi^2 c^{-\frac{2}{d}}) g_{ij}^{(k)} \text{tr} \left((C^{\text{app}})^{-1} u_k v_k^T \right) \\
&= (-2\pi^2 c^{-\frac{2}{d}}) \sum_{k \in \mathbb{Z}_N^d} \frac{\varphi(k)}{(1 - \varphi(k))^2} g_{ij}^{(k)} v_k^T (C^{\text{app}})^{-1} u_k.
\end{aligned}$$

which concludes the proof of Lemma A.2. \square

Coming back to the proof of Theorem 3.1, in the case of the Gaussian-like DPP prior, from Equations (21) and (23), Equation (20) results into

$$\nabla \log f_{\text{DPP}}^{\text{app}}(\boldsymbol{\mu} | \Lambda) = (2\pi^2 c^{-\frac{2}{d}}) \sum_{k \in \mathbb{Z}_N^d} g^{(k)} \frac{\varphi(k)}{(1 - \varphi(k))^2} \left[\frac{1 - \varphi(k)}{1 - e^{-D^{\text{app}}}} - v_k^T (C^{\text{app}})^{-1} u_k \right]$$

which concludes the proof of Theorem 3.1. \square

B Measure-Theoretic Details

From the discussion in the main text, we have that $\mathbf{y} \in \mathbb{R}^{p \times n}$, $\boldsymbol{\eta} \in \mathbb{R}^{d \times n}$, $\Sigma \in \mathbb{R}_+^p$, $\Lambda \in \mathbb{R}^{p \times d}$, $\boldsymbol{\psi} \in \mathbb{R}_+^{p \times d}$, $\boldsymbol{\phi} \in \mathbb{S}^{p \times d - 1}$ (the $pd - 1$ dimensional simplex), and $\tau \in \mathbb{R}_+$. Moreover, we consider $\boldsymbol{\mu}$ as a random point configuration, which takes values in $\Omega = \cup_{m=0}^{\infty} \Omega_m$ where Ω_m denotes the space of (pairwise distinct) m -uples of \mathbb{R}^d . We endow each Ω_m with the smallest σ -algebra which makes the following mapping measurable

$$(\mu_1, \dots, \mu_m) \mapsto \{\mu_1, \dots, \mu_m\},$$

where on the left hand side we see μ_1, \dots, μ_m as an ordered vector in R^m and on the right hand side as an unordered collection of points in R , where $R \subset \mathbb{R}^d$ is the hyper-square where μ is defined. The σ -algebra on Ω is then the smallest σ -algebra containing the union of all the σ -algebras on each Ω_m . Then, it follows that $(\boldsymbol{\mu}, \mathbf{s}, \boldsymbol{\Delta}, \mathbf{c}) \in \cup_{m=0}^{\infty} \{\Omega_m \times \mathbb{R}_+^m \times \mathcal{SP}_d^m \times \{1, \dots, m\}^n\}$, where \mathcal{SP}_d denotes the space of $d \times d$ symmetric and positive matrices.

Consider now sets $\mathfrak{Y} \subset \mathbb{R}^{p \times n}$, $\mathfrak{N} \subset R^{d \times n}$, $\Xi \subset \mathbb{R}_+^p$, $\Lambda \subset \mathbb{R}^{p \times d}$, $\Psi \subset \mathbb{R}_+^{p \times d}$, $\Phi \subset \mathbb{S}^{p \times d - 1}$, $\mathfrak{I} \subset \mathbb{R}_+$, $\mathfrak{D}_m \subset \Omega_m$, $\mathfrak{G}_m \subset \mathbb{R}_+^m$, $\mathfrak{D}_m \subset \mathcal{SP}_d^m$, $\mathfrak{C}_m \subset \{1, \dots, m\}^n$. The

dominating measure for the joint distribution of data and parameters is

$$\begin{aligned} \nu(\mathfrak{Y}) \times \mathfrak{N} \times \times \Xi \times \Lambda \times \Psi \times \Phi \times \mathfrak{T} \times \cup_{m \geq 0} \{ \mathfrak{D}_m \times \mathfrak{S}_m \times \mathfrak{D}_m \times \mathfrak{C}_m \} = \\ \int_{\mathfrak{Y}} d\mathbf{y} \times \int_{\mathfrak{N}} d\boldsymbol{\eta} \times \int_{\Xi} d\Sigma \times \int_{\Lambda} d\Lambda \times \int_{\Psi} d\boldsymbol{\psi} \times \int_{\Phi} d\boldsymbol{\phi} \times \int_{\mathfrak{T}} d\tau \times \\ \times \sum_{m=0}^{\infty} \frac{e^{-|R|}}{m!} \int_{\mathfrak{D}_m} d\boldsymbol{\mu}_m \times \int_{\mathfrak{S}_m} ds_m \times \int_{\mathfrak{D}_m} d\Delta_m \times \sum_{c_1, \dots, c_n=1}^M \mathbb{1}[\mathbf{c} \in \mathfrak{C}_m]. \end{aligned}$$

The density of data and parameters with respect to ν is given by:

$$\begin{aligned} p(\mathbf{y}, \mathbf{c}, \boldsymbol{\eta}, \boldsymbol{\mu}, \mathbf{S}, \boldsymbol{\Delta}, \Sigma, \Lambda, \boldsymbol{\psi}, \boldsymbol{\phi}, \tau) = \\ \frac{1}{T^n} \left[\prod_{i=1}^n \mathcal{N}_p(y_i | \Lambda \eta_i, \Sigma) \right] \left[\prod_{h=1}^k (S_h^{(a)})^{n_h} \text{Ga}(S_h^{(a)} | \alpha, 1) \text{IW}(\Delta_h^{(a)} | \nu_0, \Psi_0) \prod_{i:c_i=h} \mathcal{N}_d(\eta_i | \mu_h^{(a)}, \Delta_h^{(a)}) \right] \\ \left[\prod_{h=1}^{\ell} \text{Ga}(S_h^{(na)} | \alpha, 1) \text{IW}(\Delta_h^{(na)} | \nu_0, \Psi_0) \right] f_{\text{DPP}}^{\text{app}}(\boldsymbol{\mu}^{(a)} \cup \boldsymbol{\mu}^{(na)} | \rho, \Lambda, K_0; R) \\ \left[\prod_{j=1}^p \text{inv-Ga}(\sigma_j^2 | a_\sigma, b_\sigma) \prod_{h=1}^d \mathcal{N}(\lambda_{jh} | 0, \psi_{jh} \phi_{jh}^2 \tau) \text{Exp}(\Psi_{jw} | 1/2) \right] \text{Dir}(\text{vec}(\boldsymbol{\phi}) | a) \text{Ga}(\tau | pda, 1/2) \end{aligned}$$

We now introduce the auxiliary variable u such that $u | T \sim \text{Ga}(n, t)$ and consider the extended parameter space including $u \in \mathbb{R}_+$. Moreover, conditional to \mathbf{c} we split $\boldsymbol{\mu} = \boldsymbol{\mu}^{(a)} \cup \boldsymbol{\mu}^{(na)}$, $\mathbf{S} = [\mathbf{S}^{(a)}, \mathbf{S}^{(na)}]$ and $\boldsymbol{\Delta} = [\boldsymbol{\Delta}^{(a)}, \boldsymbol{\Delta}^{(na)}]$ into allocated and non-allocated components (denoted with the (a) and (na) superscript respectively). The dominating measure ν' on the extended space can be straightforwardly derived. See, for instance, Equation (17) in Beraha et al. (2022). The joint density of data and parameters with respect to ν' is then

$$\begin{aligned} p(\mathbf{y}, \mathbf{c}, \boldsymbol{\eta}, \boldsymbol{\mu}^{(a)}, \boldsymbol{\mu}^{(na)}, \mathbf{S}^{(a)}, \mathbf{S}^{(na)}, \boldsymbol{\Delta}^{(a)}, \boldsymbol{\Delta}^{(na)}, \Sigma, \Lambda, \boldsymbol{\psi}, \boldsymbol{\phi}, \tau, u) \\ = \frac{u^{n-1}}{\Gamma(n)} \left[\prod_{i=1}^n \mathcal{N}_p(y_i | \Lambda \eta_i, \Sigma) \right] \left[\prod_{h=1}^k e^{-u S_h^{(a)}} (S_h^{(a)})^{n_h} \text{Ga}(S_h^{(a)} | \alpha, 1) \text{IW}(\Delta_h^{(a)} | \nu_0, \Psi_0) \right. \\ \left. \times \prod_{i:c_i=h} \mathcal{N}_d(\eta_i | \mu_h^{(a)}, \Delta_h^{(a)}) \right] \left[\prod_{h=1}^{\ell} e^{-u S_h^{(na)}} \text{Ga}(S_h^{(na)} | \alpha, 1) \text{IW}(\Delta_h^{(na)} | \nu_0, \Psi_0) \right] \\ f_{\text{DPP}}^{\text{app}}(\boldsymbol{\mu}^{(a)} \cup \boldsymbol{\mu}^{(na)} | \rho, \Lambda, K_0; R) \prod_{j=1}^p \left[\text{inv-Ga}(\sigma_j^2 | a_\sigma, b_\sigma) \prod_{h=1}^d \mathcal{N}(\lambda_{jh} | 0, \psi_{jh} \phi_{jh}^2 \tau) \right. \\ \left. \times \prod_{h=1}^d \text{Exp}(\Psi_{jd} | 1/2) \right] \text{Dir}(\text{vec}(\boldsymbol{\phi}) | a) \text{Ga}(\tau | pda, 1/2). \end{aligned}$$

C The Anisotropic Whittle-Matérn DPP

Corollary C.1. *Using the same notation of Theorem 2.1, let*

$$W \sim \text{Gamma}\left(\nu + \frac{d}{2}, \frac{1}{2|\Lambda^T \Lambda|^{\frac{1}{d}} \alpha^2}\right), \quad \nu, \alpha > 0,$$

where Λ is fixed. Then the kernel K_0 , its Fourier transform $\varphi = \mathcal{F}(K_0)$ and ρ_{\max} follow here:

$$\begin{aligned} K_0(x) &= \rho \frac{2^{1-\nu}}{\Gamma(\nu)} \left\| \frac{\Lambda x}{\alpha |\Lambda^T \Lambda|^{\frac{1}{2d}}} \right\|^\nu K_\nu \left(\left\| \frac{\Lambda x}{\alpha |\Lambda^T \Lambda|^{\frac{1}{2d}}} \right\| \right), \quad x \in \mathbb{R}^d \\ \varphi(x) &= \rho \frac{\Gamma(\nu + \frac{d}{2})}{\Gamma(\nu)} \frac{(2\sqrt{\pi}\alpha)^d}{(1 + 4\pi^2 \alpha^2 |\Lambda^T \Lambda|^{\frac{1}{d}} x^T (\Lambda^T \Lambda)^{-1} x)^{\nu + \frac{d}{2}}}, \quad x \in \mathbb{R}^d \\ \rho_{\max} &= \frac{\Gamma(\nu)}{\Gamma(\nu + \frac{d}{2}) (2\sqrt{\pi}\alpha)^d} \end{aligned} \quad (27)$$

where K_ν is the modified Bessel function of the second kind.

Proof. Let $\nu > 0$ and $\alpha > 0$. In Theorem 2.1, set

$$W \sim \text{Gamma}\left(\nu + \frac{d}{2}, \frac{1}{2|\Lambda^T \Lambda|^{\frac{1}{d}} \alpha^2}\right).$$

Applying Equation (18), we explicitly compute $h(x)$ as

$$\begin{aligned} h(x) &= \frac{|\Lambda^T \Lambda|^{\frac{1}{2}}}{(2\pi)^{\frac{d}{2}}} \int_0^{+\infty} \left[w^{-\frac{d}{2}} \exp\left(-\frac{\|\Lambda x\|^2}{2w}\right) \left(\frac{1}{2|\Lambda^T \Lambda|^{\frac{1}{d}} \alpha^2}\right)^{\nu + \frac{d}{2}} \frac{w^{\nu + \frac{d}{2} - 1}}{\Gamma(\nu + \frac{d}{2})} \right. \\ &\quad \left. \cdot \exp\left(-\frac{w}{2|\Lambda^T \Lambda|^{\frac{1}{d}} \alpha^2}\right) \right] dw = \\ &= \frac{|\Lambda^T \Lambda|^{-\frac{\nu}{d}}}{(2\pi)^{\frac{d}{2}} (2\alpha^2)^{\nu + \frac{d}{2}} \Gamma(\nu + \frac{d}{2})} \int_0^{+\infty} w^{\nu-1} \exp\left[-\frac{1}{2} \left(\frac{1}{|\Lambda^T \Lambda|^{\frac{1}{d}} \alpha^2} w + \frac{\|\Lambda x\|^2}{w}\right)\right] dw. \end{aligned}$$

In this paper, by generalized inverse Gaussian distribution (GIG) on $[0, +\infty)$ with parameters (p, a, b) we mean an absolutely continuous distribution with density

$$f(x) = \frac{(a/b)^{\frac{p}{2}}}{2K_p(\sqrt{ab})} x^{p-1} \exp\left(-\frac{1}{2} \left[ax + \frac{b}{x}\right]\right), \quad x > 0 \quad (28)$$

where $p \in \mathbb{R}$, $a > 0$ and $b > 0$. In the above expression K_p is the modified Bessel function of the second kind. We indicate such a distribution with $\text{giG}(p, a, b)$.

Coming back to the computation of $h(x)$, we see in the last integral that the integrand is the density of a generalized inverse Gaussian distribution with parameters

$$p = \nu, \quad a = \frac{1}{|\Lambda^T \Lambda|^{\frac{1}{d}} \alpha^2}, \quad b = \|\Lambda x\|^2$$

Therefore,

$$\begin{aligned} h(x) &= \frac{|\Lambda^T \Lambda|^{-\frac{\nu}{d}}}{(2\pi)^{\frac{d}{2}} (2\alpha^2)^{\nu + \frac{d}{2}} \Gamma(\nu + \frac{d}{2})} \cdot \left(|\Lambda^T \Lambda|^{\frac{1}{d}} \alpha^2 \|\Lambda x\|^2 \right)^{\frac{\nu}{2}} \cdot 2 K_\nu \left(\frac{\|\Lambda x\|}{|\Lambda^T \Lambda|^{\frac{1}{2d}} \alpha} \right) \\ &= \frac{1}{(\sqrt{\pi} \alpha)^d 2^{\nu+d-1} \Gamma(\nu + \frac{d}{2})} \cdot \left\| \frac{\Lambda x}{\alpha |\Lambda^T \Lambda|^{\frac{1}{2d}}} \right\|^\nu \cdot K_\nu \left(\left\| \frac{\Lambda x}{\alpha |\Lambda^T \Lambda|^{\frac{1}{2d}}} \right\| \right). \end{aligned}$$

Note that, as $x \rightarrow 0$, then $x^\nu K_\nu(x) \rightarrow 2^{\nu-1} \Gamma(\nu)$. Consequently, the kernel K_0 is

$$K_0(x) = \rho \frac{2^{1-\nu}}{\Gamma(\nu)} \cdot \left\| \frac{\Lambda x}{\alpha |\Lambda^T \Lambda|^{\frac{1}{2d}}} \right\|^\nu \cdot K_\nu \left(\left\| \frac{\Lambda x}{\alpha |\Lambda^T \Lambda|^{\frac{1}{2d}}} \right\| \right).$$

To derive the spectral density $\varphi = \mathcal{F}(K_0)$, from (9) we have

$$\begin{aligned} \varphi(x) &= \frac{\rho}{h(0)} \int_0^\infty \exp(-2\pi^2 w x^T (\Lambda^T \Lambda)^{-1} x) \left(\frac{1}{2|\Lambda^T \Lambda|^{\frac{1}{d}} \alpha^2} \right)^{\nu + \frac{d}{2}} \frac{w^{\nu + \frac{d}{2} - 1}}{\Gamma(\nu + \frac{d}{2})} \exp\left(-\frac{w}{2|\Lambda^T \Lambda|^{\frac{1}{d}} \alpha^2}\right) dw \\ &= \frac{\rho}{h(0) (2|\Lambda^T \Lambda|^{\frac{1}{d}} \alpha^2)^{\nu + \frac{d}{2}}} \int_0^\infty \frac{w^{\nu + \frac{d}{2} - 1}}{\Gamma(\nu + \frac{d}{2})} \exp\left[-\left(2\pi^2 x^T (\Lambda^T \Lambda)^{-1} x + \frac{1}{2|\Lambda^T \Lambda|^{\frac{1}{d}} \alpha^2}\right) w\right] dw \\ &= \frac{\rho}{h(0) (2|\Lambda^T \Lambda|^{\frac{1}{d}} \alpha^2)^{\nu + \frac{d}{2}}} \cdot \frac{1}{\left(2\pi^2 x^T (\Lambda^T \Lambda)^{-1} x + \frac{1}{2|\Lambda^T \Lambda|^{\frac{1}{d}} \alpha^2}\right)^{\nu + \frac{d}{2}}} \\ &= \frac{\rho}{h(0)} \cdot \frac{1}{\left(1 + 4\pi^2 \alpha^2 |\Lambda^T \Lambda|^{\frac{1}{d}} x^T (\Lambda^T \Lambda)^{-1} x\right)^{\nu + \frac{d}{2}}}, \end{aligned}$$

so that the spectral density $\varphi = \mathcal{F}(K_0)$ is

$$\varphi(x) = \rho \frac{\Gamma(\nu + \frac{d}{2})}{\Gamma(\nu)} \frac{(2\sqrt{\pi} \alpha)^d}{\left(1 + 4\pi^2 \alpha^2 |\Lambda^T \Lambda|^{\frac{1}{d}} x^T (\Lambda^T \Lambda)^{-1} x\right)^{\nu + \frac{d}{2}}}.$$

To sum up, we report the kernel K_0 and the spectral density φ of this model

$$\begin{aligned} K_0(x) &= \rho \frac{2^{1-\nu}}{\Gamma(\nu)} \cdot \left\| \frac{\Lambda x}{\alpha |\Lambda^T \Lambda|^{\frac{1}{2d}}} \right\|^\nu \cdot K_\nu \left(\left\| \frac{\Lambda x}{\alpha |\Lambda^T \Lambda|^{\frac{1}{2d}}} \right\| \right) \\ \varphi(x) &= \rho \frac{\Gamma(\nu + \frac{d}{2})}{\Gamma(\nu)} \frac{(2\sqrt{\pi} \alpha)^d}{\left(1 + 4\pi^2 \alpha^2 |\Lambda^T \Lambda|^{\frac{1}{d}} x^T (\Lambda^T \Lambda)^{-1} x\right)^{\nu + \frac{d}{2}}}. \end{aligned}$$

The existence condition, from Equation (7), requires $\rho \leq \rho_{max}$, with

$$\rho_{max} = \frac{\Gamma(\nu)}{\Gamma(\nu + \frac{d}{2}) (2\sqrt{\pi}\alpha)^d}.$$

□

We now show how to compute analytically the gradient of the full conditional for Λ also in the case of Whittle-Matérn DPP prior.

Theorem C.2. *Under the Whittle-Matérn-like DPP prior, the gradient of the log-full conditional density of Λ equals*

$$\begin{aligned} \nabla \log p(\Lambda \mid \dots) &= \Sigma^{-1} \sum_{i=1}^n (y_i - \Lambda \eta_i) \eta_i^\top + \\ &\quad + 4\pi^2 \alpha^2 \left(\nu + \frac{d}{2} \right) \sum_{k \in \mathbb{Z}_N^d} \frac{g^{(k)}}{a^{(k)}} \frac{\varphi(k)}{(1 - \varphi(k))^2} \left[\frac{1 - \varphi(k)}{1 - e^{-D^{\text{app}}}} - v_k^\top (C^{\text{app}})^{-1} u_k \right] + \\ &\quad - \frac{1}{(\psi \odot \phi^2) \tau^2} \odot \Lambda \end{aligned}$$

where $\varphi(k)$ is defined in (27), \odot denotes the elementwise (Hadamard) product,

$$g^{(k)} = 2|\Lambda^T \Lambda|^{\frac{1}{d}} \Lambda (\Lambda^T \Lambda)^{-1} \left[\frac{1}{d} k^T (\Lambda^T \Lambda)^{-1} k \mathbf{1}_d - k ((\Lambda^T \Lambda)^{-1} k)^T \right],$$

u_k and v_k are m -dimensional column vectors for each $k \in \mathbb{Z}^d$ with entries

$$(u_k)_j = e^{2\pi i k^T T \mu_j}, \quad (v_k)_j = e^{-2\pi i k^T T \mu_j}, \quad j = 1, \dots, m$$

$C^{\text{app}} := C^{\text{app}}(T\mu_1, \dots, T\mu_n)$, and $a^{(k)} = 1 + 4\pi^2 \alpha^2 |\Lambda^T \Lambda|^{\frac{1}{d}} k^T (\Lambda^T \Lambda)^{-1} k$.

Proof. The proof follows closely the one of Theorem 3.1. Instead of Lemma A.1 and Lemma A.2, we use the two following results

Lemma C.3. *For the Whittle-Matérn-like DPP prior,*

$$\nabla D^{\text{app}} = \sum_{k \in \mathbb{Z}_N^d} \frac{\varphi(k)}{1 - \varphi(k)} 4\pi^2 \alpha^2 \left(-\nu - \frac{d}{2} \right) \frac{g^{(k)}}{a^{(k)}} \quad (29)$$

where $\varphi(k)$ refers to (27).

Proof. Write

$$\nabla D^{\text{app}} = - \sum_{k \in \mathbb{Z}_N^d} \nabla \log(1 - \varphi(k)) = \sum_{k \in \mathbb{Z}_N^d} \frac{1}{1 - \varphi(k)} \nabla \varphi(k).$$

For the Whittle-Matérn-like DPP prior, from (27), observe that, for $k \in \mathbb{Z}^d$

$$\begin{aligned}\nabla\varphi(k) &= \rho \frac{\Gamma(\nu + \frac{d}{2})}{\Gamma(\nu)} (2\sqrt{\pi}\alpha)^d \nabla \left((1 + 4\pi^2\alpha^2 |\Lambda^T \Lambda|^{\frac{1}{d}} k^T (\Lambda^T \Lambda)^{-1} k)^{-\nu - \frac{d}{2}} \right) \\ &= \frac{\varphi(k)}{a^{(k)}} 4\pi^2\alpha^2 \left(-\nu - \frac{d}{2} \right) \nabla \left(|\Lambda^T \Lambda|^{\frac{1}{d}} k^T (\Lambda^T \Lambda)^{-1} k \right).\end{aligned}$$

Note that

$$\begin{aligned}\nabla \left(|\Lambda^T \Lambda|^{\frac{1}{d}} k^T (\Lambda^T \Lambda)^{-1} k \right) &= \nabla \left(|\Lambda^T \Lambda|^{\frac{1}{d}} \right) k^T (\Lambda^T \Lambda)^{-1} k + \\ &\quad + |\Lambda^T \Lambda|^{\frac{1}{d}} \nabla \left(k^T (\Lambda^T \Lambda)^{-1} k \right) = \\ &= \frac{1}{d} |\Lambda^T \Lambda|^{\frac{1}{d}-1} 2 |\Lambda^T \Lambda| \Lambda (\Lambda^T \Lambda)^{-1} k^T (\Lambda^T \Lambda)^{-1} k + \\ &\quad + |\Lambda^T \Lambda|^{\frac{1}{d}} \nabla \left(k^T (\Lambda^T \Lambda)^{-1} k \right)\end{aligned}$$

where, in the last step, formula (53) of Petersen & Pedersen (2008) is used. Then,

$$\begin{aligned}\nabla \left(k^T (\Lambda^T \Lambda)^{-1} k \right) &= \nabla \text{tr} \left(k^T (\Lambda^T \Lambda)^{-1} k \right) = \\ &= \nabla \text{tr} \left((\Lambda^T \Lambda)^{-1} k k^T \right) = -\Lambda (\Lambda^T \Lambda)^{-1} (2k k^T) (\Lambda^T \Lambda)^{-1}\end{aligned}$$

where, in the last step, we have applied formula (125) of Petersen & Pedersen (2008). For the Whittle-Matérn-like DPP prior, it follows

$$\nabla\varphi(k) = \frac{\varphi(k)}{a^{(k)}} 8\pi^2\alpha^2 \left(-\nu - \frac{d}{2} \right) |\Lambda^T \Lambda|^{\frac{1}{d}} \Lambda (\Lambda^T \Lambda)^{-1} \left[\frac{1}{d} k^T (\Lambda^T \Lambda)^{-1} k \mathbb{1}_d - k k^T (\Lambda^T \Lambda)^{-1} \right]$$

where $\mathbb{1}_d$ is $d \times d$ matrix of 1's. This concludes the proof of Lemma C.3. \square

Lemma C.4. *For the Whittle-Matérn-like DPP prior,*

$$\nabla \log \det[C^{\text{app}}] = 4\pi^2\alpha^2 \left(-\nu - \frac{d}{2} \right) \sum_{k \in \mathbb{Z}_N^d} \frac{\varphi(k)}{(1 - \varphi(k))^2} \frac{g^{(k)}}{a^{(k)}} v_k^T (C^{\text{app}})^{-1} u_k \quad (30)$$

where $\varphi(k)$ refers to (27).

Proof. Proceeding as in the proof of Lemma C.4, we have

$$\frac{\partial}{\partial \Lambda_{ij}} \log \det[C^{\text{app}}] = \text{tr} \left(\left(\frac{\partial}{\partial U} \log \det U \right) \Big|_{U=C^{\text{app}}} \cdot \frac{\partial}{\partial \Lambda_{ij}} C^{\text{app}} \right) \quad (31)$$

$$\begin{aligned}&= \text{tr} \left(\frac{1}{\det[C^{\text{app}}]} \left(\frac{\partial}{\partial U} \det U \right) \Big|_{U=C^{\text{app}}} \cdot \frac{\partial}{\partial \Lambda_{ij}} C^{\text{app}} \right) \\ &= \text{tr} \left((C^{\text{app}})^{-1} \cdot \frac{\partial}{\partial \Lambda_{ij}} C^{\text{app}} \right)\end{aligned} \quad (32)$$

where formula (137) of Petersen & Pedersen (2008) is used to get Equation (31) and formula (49) of Petersen & Pedersen (2008) for Equation (32). Now, note that

$$C^{\text{app}} = \sum_{k \in \mathbb{Z}_N^d} \frac{\varphi(k)}{1 - \varphi(k)} u_k v_k^T \quad (33)$$

where u_k, v_k are defined in the statement. It follows that, for the Whittle-Matérn-like DPP prior,

$$\frac{\partial}{\partial \Lambda_{ij}} C^{\text{app}} = \sum_{k \in \mathbb{Z}_N^d} \frac{\varphi(k)}{(1 - \varphi(k))^2} 4\pi^2 \alpha^2 \left(-\nu - \frac{d}{2} \right) \frac{g_{ij}^{(k)}}{a^{(k)}} u_k v_k^T.$$

Then, back to Equation (32), for the Whittle-Matérn-like DPP prior,

$$\frac{\partial}{\partial \Lambda_{ij}} \log \det[C^{\text{app}}] = 4\pi^2 \alpha^2 \left(-\nu - \frac{d}{2} \right) \sum_{k \in \mathbb{Z}_N^d} \frac{\varphi(k)}{(1 - \varphi(k))^2} \frac{g_{ij}^{(k)}}{a^{(k)}} v_k^T (C^{\text{app}})^{-1} u_k$$

which concludes the proof of Lemma C.4 \square

Coming back to the proof of Theorem C.2, in the case of the Whittle-Matérn-like DPP prior, from Equations (29) and (30), Equation (20) results into

$$\nabla \log f_{\text{DPP}}^{\text{app}}(\boldsymbol{\mu} | \Lambda) = 4\pi^2 \alpha^2 \left(\nu + \frac{d}{2} \right) \sum_{k \in \mathbb{Z}_N^d} \frac{g^{(k)}}{a^{(k)}} \frac{\varphi(k)}{(1 - \varphi(k))^2} \left[\frac{1 - \varphi(k)}{1 - e^{-D^{\text{app}}}} - v_k^T (C^{\text{app}})^{-1} u_k \right]$$

which concludes the proof of Theorem C.2. \square

D Further details on the MCMC algorithm

D.1 The Gibbs Sampler

Here below we summarize the steps of our Gibbs sampler, though calculation of the full conditionals is omitted when it is straightforward.

1. *Update of (ψ, τ, ϕ) .* Following Bhattacharya et al. (2015) sample

$$\begin{aligned} \psi_{jh} | \lambda_{jh}, \phi_{jh}, \tau &\stackrel{\text{ind}}{\sim} \text{giG} \left(\frac{1}{2}, 1, \frac{\lambda_{jh}^2}{\phi_{jh}^2 \tau^2} \right) \\ \tau | \phi, \Lambda &\sim \text{giG} \left(p \cdot d \cdot (a - 1), 1, 2 \sum_{\substack{j=1:p \\ h=1:d}} \frac{|\lambda_{jh}|}{\phi_{jh}} \right) \\ \phi_{jh} = \frac{T_{jh}}{T}, \quad T_{jh} &\stackrel{\text{ind}}{\sim} \text{giG}(a - 1, 1, 2|\lambda_{jh}|), \quad T := \sum_{j,h} T_{jh}, \end{aligned}$$

for $j = 1, \dots, p, h = 1, \dots, d$, where giG denotes the generalized inverse-Gaussian distribution (see (28)).

2. *Update of Λ .* Sample from the full conditional density

$$p(\Lambda \mid \cdots) \propto p(\mathbf{y} \mid \Lambda, \boldsymbol{\eta}, \Sigma) p(\Lambda \mid \phi, \tau, \psi) f_{\text{DPP}}^{\text{app}}(\boldsymbol{\mu} \mid \rho, \Lambda, K_0; R)$$

using a Metropolis-Hastings step; see Section 3.3 for further details.

3. *Update of Σ .* Sample each σ_j^2 independently from

$$\sigma_j^2 \mid \mathbf{y}^{(j)}, \boldsymbol{\eta}, \lambda^{(j)} \stackrel{\text{ind}}{\sim} \text{inv - Gamma} \left(\frac{n}{2} + a_\sigma, \frac{1}{2} \sum_{i=1}^n \left(y_i^{(j)} - \lambda^{(j)T} \eta_i \right)^2 + b_\sigma \right)$$

where $\lambda^{(j)\top}$ is the j -th row of Λ and $\mathbf{y}^{(j)} = (y_{1j}, \dots, y_{nj})^\top$.

4. *Update of the non-allocated variables $(\boldsymbol{\mu}^{(na)}, \mathbf{s}^{(na)}, \boldsymbol{\Delta}^{(na)})$.* Following Beraha et al. (2022), we disintegrate the joint full conditional of the non-allocated variables as

$$p(\boldsymbol{\mu}^{(na)}, \mathbf{s}^{(na)}, \boldsymbol{\Delta}^{(na)} \mid \text{rest}) = p(\boldsymbol{\mu}^{(na)} \mid \text{rest}) p(\mathbf{s}^{(na)} \mid \boldsymbol{\mu}^{(na)}, \text{rest}) p(\boldsymbol{\Delta}^{(na)} \mid \boldsymbol{\mu}^{(na)}, \text{rest}),$$

where “rest” identifies all the variables except for $(\boldsymbol{\mu}^{(na)}, \mathbf{s}^{(na)}, \boldsymbol{\Delta}^{(na)})$. Then $\boldsymbol{\mu}^{(na)} \mid \text{rest}$ is a Gibbs point process with density

$$p(\{\mu_1^{(na)}, \dots, \mu_\ell^{(na)}\} \mid \text{rest}) \propto f_{\text{DPP}}^{\text{app}}(\{\mu_1^{(na)}, \dots, \mu_\ell^{(na)}\} \cup \boldsymbol{\mu}^{(a)} \mid \rho, \Lambda, K_0; R) \psi(u)^\ell$$

where $\psi(u) = \mathbb{E}[e^{-uS}]$. We employ the birth-death Metropolis-Hastings algorithm in Geyer & Møller (1994) to sample from this point process density. Given $\boldsymbol{\mu}^{(na)}$ it is straightforward to show

$$\begin{aligned} \Delta_1^{(na)}, \dots, \Delta_\ell^{(na)} \mid \dots &\stackrel{\text{iid}}{\sim} \text{IW}_d(\nu_0, \Psi_0) \\ S_1^{(na)}, \dots, S_\ell^{(na)} \mid \dots &\stackrel{\text{iid}}{\sim} \text{Gamma}(\alpha, 1 + u) \end{aligned}$$

5. *Update of the allocated variables $(\boldsymbol{\mu}^{(a)}, \mathbf{s}^{(a)}, \boldsymbol{\Delta}^{(a)})$.* Let k be the number of unique values in the allocation vector \mathbf{c} and assume that the active components are the first k . We can sample the allocated variables using a Gibbs scan. It is trivial to show that

$$\begin{aligned} S_h^{(a)} \mid \dots &\stackrel{\text{ind}}{\sim} \text{Gamma}(\alpha + n_h, 1 + u) \\ \Delta_h^{(a)} \mid \dots &\stackrel{\text{ind}}{\sim} \text{IW}_d \left(\nu_0 + n_h, \Psi_0 + \sum_{i:c_i=h} (\eta_i - \mu_h^{(a)})(\eta_i - \mu_h^{(a)})^\top \right). \end{aligned}$$

The full conditional of $\boldsymbol{\mu}^{(a)}$ is proportional to

$$p(\boldsymbol{\mu}^{(a)} \mid \cdots) \propto f_{\text{DPP}}^{\text{app}}(\boldsymbol{\mu}^{(a)} \cup \boldsymbol{\mu}^{(na)} \mid \rho, \Lambda, K_0; R) \prod_{h=1}^k \prod_{i:c_i=h} \mathcal{N}_d(\eta_i \mid \mu_h^{(a)}, \Delta_h^{(a)})$$

and we use a Metropolis-Hastings step to sample from it.

6. *Update of the latent allocation variables c .* We found it useful to marginalize over the η_i 's to get better mixing chains. Hence, we can sample each c_i independently from a discrete distribution over $\{1, \dots, k + \ell\}$ with weights ω_{ih} :

$$\begin{aligned}\omega_{ih} &\propto S_h^{(a)} \mathcal{N}_p(y_i | \Lambda \mu_h^{(a)}, \Sigma + \Lambda \Delta_h^{(a)} \Lambda^\top), & h = 1, \dots, k \\ \omega_{ik+h} &\propto S_h^{(na)} \mathcal{N}_p(y_i | \Lambda \mu_h^{(na)}, \Sigma + \Lambda \Delta_h^{(na)} \Lambda^\top), & h = 1, \dots, \ell\end{aligned}$$

Each evaluation of the p -dimensional Gaussian density would require $\mathcal{O}(p^3)$ operations if care is not taken. However, we take advantage from the special structure of the covariance matrix. Using Woodbury's matrix identity, we have that

$$(\Sigma + \Lambda \Delta \Lambda^\top)^{-1} = \Sigma^{-1} - \Sigma^{-1} \Lambda (\Delta^{-1} + \Lambda^\top \Sigma^{-1} \Lambda)^{-1} \Lambda^\top \Sigma^{-1},$$

and hence we need now to compute the inverse of a $d \times d$ matrix. Therefore, evaluating the quadratic form in the exponential requires only $\mathcal{O}(p)$ computational cost. Moreover, using the matrix determinant lemma, the determinant of the covariance matrix can be computed as

$$\det(\Sigma + \Lambda \Delta \Lambda^\top) = \det(\Delta^{-1} + \Lambda^\top \Sigma^{-1} \Lambda) \det(\Delta) \det(\Sigma).$$

This is computed without additional cost by caching operations from the previous matrix inversion.

7. *Update of the ancillary variable $u \sim \text{Gamma}(n, T)$.*
 8. *Update of the latent scores η .* For $i = 1, \dots, n$, sample each η_i independently from

$$\eta_i | \dots \stackrel{\text{ind}}{\sim} \mathcal{N}_d(m_i, S_i)$$

where

$$S_i = \left(\Lambda^T \Sigma^{-1} \Lambda + (\Delta_{c_i}^{(a)})^{-1} \right)^{-1}, \quad m_i = S_i \left(\Lambda^T \Sigma^{-1} y_i + (\Delta_{c_i}^{(a)})^{-1} \mu_{c_i}^{(a)} \right)$$

This follows by standard calculations.

D.2 Analytical approach vs Automatic Differentiation

In Figure 5, we report the comparison, in terms of memory usage (measured in Bytes) and execution time per iteration (measured in seconds), between the AD approach and the analytical approach in sampling the high-dimensional matrix of loadings Λ . Fixing all the other model parameters, we set $N = 4$ and 6 component centers μ_h 's; see also Equation (15). Note that the value of N impacts on both the memory usage and the execution time. We compare the performance in sampling only the matrix Λ . We use 100 data points simulated from a p -dimensional Gaussian distribution, for $p = 100, 200$.

D.3 Mixing of the Lamb algorithm

Figure 6 shows the chain of the number of clusters produced by the Lamb algorithm along the iterations. We perform 10^5 iterations and we plot one every ten iterations. We use the data of simulation study B, with $p = 100$, $d = 5$ and set $\alpha_{DP} = 0.5$. Note that the chain has not reached convergence yet after 10^5 iterations, demanding a very long burn-in phase. The poor efficiency of the Lamb algorithm is common in all the settings analyzed in our simulation studies.

D.4 Gibbs Sampler for binary data

The Gibbs sampler here requires an additional step to deal with the binary observations $z_{i,j}$. Specifically, the Gibbs updates described for the original APPLAM model, i.e., steps 1-8, except for the parameters here fixed, can be applied, since all the involved parameters are independent of $\mathbf{z} = (z_1, \dots, z_n)$, conditionally to $\mathbf{y} = (y_1, \dots, y_n)$. Then, the update of the y_i 's is done as follows:

$$y_{i,j} \mid z_{i,j}, \dots \stackrel{\text{ind}}{\sim} \begin{cases} \mathcal{N}(y_{i,j} \mid (\Lambda\eta_i)_j, 1) \mathbb{1}_{[0,\infty)}(y_{i,j}), & \text{if } z_{i,j} = 1; \\ \mathcal{N}(y_{i,j} \mid (\Lambda\eta_i)_j, 1) \mathbb{1}_{(-\infty,0)}(y_{i,j}), & \text{if } z_{i,j} = 0, \end{cases}$$

for $i = 1, \dots, n; j = 1, \dots, p$, where $(\Lambda\eta_i)_j$ indicates the j -th element of the p -dimensional vector $\Lambda\eta_i$. That is, if $z_{i,j} = 1$ (resp. $z_{i,j} = 0$) the full-conditional distribution of $y_{i,j}$ follows a truncated Gaussian distribution with support $[0, \infty)$ (resp. support $(-\infty, 0)$).

E Details on simulations

E.1 Details on synthetic data simulation

In this section, we describe the values μ_h , $h = 1, \dots, M$, $M = 4$, and Λ to simulate the data in both simulation studies. We fix $\mu_1 = \{7.5\}^d$, $\mu_2 = \{2.5\}^d$, $\mu_3 = \{-2.5\}^d$ and $\mu_4 = \{-7.5\}^d$. The matrix of factor loadings Λ is set as follows. Let e_k , $k = 1, \dots, d$, be the standard basis of \mathbb{R}^d , then Λ is built by stacking by row these basis vectors as: repeat e_1 for c times, ... , e_{d-1} for c times, e_d for $p - c(d - 1)$ times, so that $p - c(d - 1) < c$.

E.2 Default values for the hyperparameters

We follow Chandra et al. (2020) for all the hyperparameters that are shared between Lamb and APPLAM. Specifically, we set $a_\sigma = 1$, $b_\sigma = 0.3$ in (13) and $a = 0.5$ in (14). Moreover, Lamb assumes a Dirichlet process location-scale mixture of Gaussian densities for the latent factors. In particular, the Normal-inverseWishart distribution is taken as base measure, with location μ_0 , scale k , covariance matrix Ψ_0 and degrees of freedom ν_0 . The default choice sets μ_0 as the null vector, $k = 0.001$, $\Psi_0 = \delta I_d$, with $\delta = 20$ and $\nu_0 = d + 50$. Coherently, for APPLAM we set $\Psi_0 = \delta I_d$, $\delta = 20$ and $\nu_0 = d + 50$ in (12). We also set $\alpha = 1$ in (16).

E.3 Additional tables and plots

This section also reports the summary statistics for the cluster analysis in the two simulations discussed in Section 4 of the main paper. See Tables 1 - 6.

d	Model	Parameter	MODE NCLUS	MEAN NCLUS	ARI BEST	CI ARI
2	Lamb	0.1	5	4.76	0.94	[0.953, 0.955]
		0.5	5	5.26	0.94	[0.932, 0.934]
		1.0	28	27.61	0.22	[0.268, 0.27]
	APPLAM	5.0	6	6.64	0.83	[0.824, 0.829]
		10.0	9	9.02	0.72	[0.717, 0.725]
		20.0	6	6.07	0.91	[0.883, 0.889]
5	Lamb	0.1	54	54.27	0.09	[0.099, 0.1]
		0.5	62	62.65	0.08	[0.081, 0.081]
		1.0	41	39.70	0.34	[0.354, 0.355]
	APPLAM	5.0	4	4.01	1.00	[1.0, 1.0]
		10.0	4	4.02	1.00	[1.0, 1.0]
		20.0	4	4.00	1.00	[1.0, 1.0]
8	Lamb	0.1	38	39.17	0.73	[0.734, 0.735]
		0.5	30	30.42	0.68	[0.67, 0.67]
		1.0	31	31.00	0.75	[0.751, 0.751]
	APPLAM	5.0	4	4.02	1.00	[1.0, 1.0]
		10.0	4	4.00	1.00	[1.0, 1.0]
		20.0	4	4.00	1.00	[1.0, 1.0]

Table 1: Simulation study A, $p = 100$: posterior modes and means of the number of clusters, the ARI between the estimated partition and the true one, credible intervals for the ARI between the random and true partition of the data with different values of the hyperparameters.

d	Model	Parameter	MODE NCLUS	MEAN NCLUS	ARI BEST	CI ARI
2	Lamb	0.1	6	5.85	0.92	[0.901, 0.905]
		0.5	27	27.20	0.27	[0.254, 0.256]
		1.0	30	29.79	0.24	[0.238, 0.239]
	APPLAM	5.0	6	6.28	0.86	[0.822, 0.825]
		10.0	6	6.41	0.84	[0.837, 0.84]
		20.0	7	6.92	0.85	[0.837, 0.841]
5	Lamb	0.1	66	68.96	0.06	[0.068, 0.068]
		0.5	69	70.11	0.06	[0.068, 0.069]
		1.0	65	68.00	0.06	[0.072, 0.072]
	APPLAM	5.0	4	4.01	1.00	[1.0, 1.0]
		10.0	4	4.01	1.00	[1.0, 1.0]
		20.0	4	4.00	1.00	[1.0, 1.0]
8	Lamb	0.1	39	39.93	0.23	[0.228, 0.229]
		0.5	38	40.82	0.23	[0.238, 0.239]
		1.0	62	61.84	0.11	[0.108, 0.109]
	APPLAM	5.0	4	4.00	1.00	[1.0, 1.0]
		10.0	4	4.00	1.00	[1.0, 1.0]
		20.0	4	4.00	1.00	[1.0, 1.0]

Table 2: Simulation study A, $p = 200$: posterior modes and means of the number of clusters, the ARI between the estimated partition and the true one, credible intervals for the ARI between the random and true partition of the data with different values of the hyperparameters.

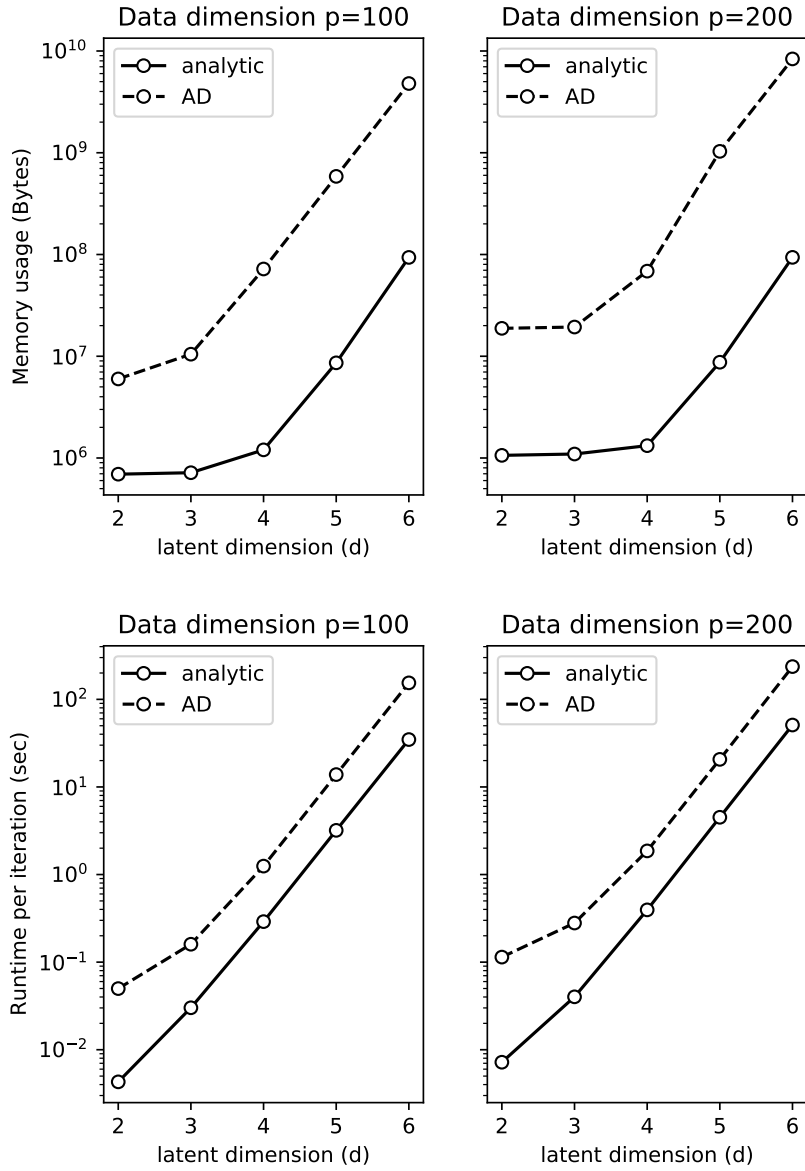


Figure 5: Memory requirement (top row) and run-time execution per iteration of MCMC with $n = 100$ samples when the data-dimension is $p = 100$ (left plot) and $p = 200$ (right plot) as the latent dimension d varies.

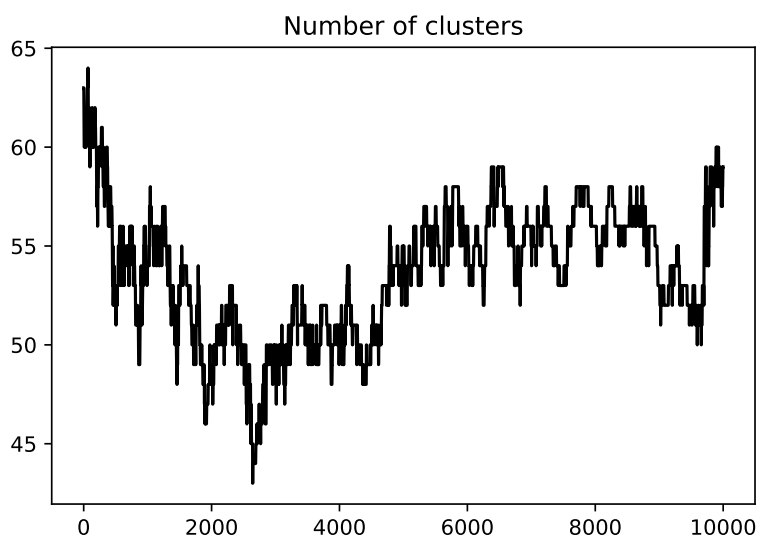


Figure 6: Traceplot of the number of clusters produced by the Lamb algorithm for 10^5 iterations for simulation study B, with $p = 100$, $d = 5$ and we set $\alpha_{DP} = 0.5$

d	Model	Parameter	MODE NCLUS	MEAN NCLUS	ARI BEST	CI ARI
2	Lamb	0.1	10	9.97	0.72	[0.716, 0.72]
		0.5	37	37.02	0.19	[0.194, 0.195]
		1.0	39	38.98	0.20	[0.185, 0.186]
	APPLAM	5.0	6	5.67	0.60	[0.596, 0.599]
		10.0	8	7.86	0.79	[0.795, 0.799]
		20.0	6	5.99	0.80	[0.709, 0.721]
5	Lamb	0.1	84	83.43	0.05	[0.051, 0.051]
		0.5	85	85.25	0.05	[0.051, 0.051]
		1.0	86	86.09	0.05	[0.05, 0.051]
	APPLAM	5.0	4	3.77	1.00	[0.852, 0.873]
		10.0	4	4.36	1.00	[0.99, 0.992]
		20.0	4	4.12	1.00	[0.989, 0.991]
8	Lamb	0.1	75	74.37	0.07	[0.075, 0.075]
		0.5	73	72.34	0.08	[0.079, 0.079]
		1.0	76	76.51	0.08	[0.083, 0.083]
	APPLAM	5.0	4	4.00	1.00	[1.0, 1.0]
		10.0	4	4.00	1.00	[1.0, 1.0]
		20.0	4	4.00	1.00	[1.0, 1.0]

Table 3: Simulation study A, $p = 400$: posterior modes and means of the number of clusters, the ARI between the estimated partition and the true one, credible intervals for the ARI between the random and true partition of the data with different values of the hyperparameters.

Latent dim	Model	Parameter	mode_nclus	avg_nclus	ari_best_clus	CI_aris
2	Lamb	0.1	7	7.29	0.87	[0.857, 0.858]
		0.5	8	7.90	0.87	[0.858, 0.859]
		1.0	8	8.29	0.88	[0.86, 0.861]
	APPLAM	5.0	8	8.53	0.68	[0.657, 0.662]
		10.0	11	11.12	0.50	[0.513, 0.518]
		20.0	9	9.50	0.66	[0.633, 0.639]
5	Lamb	0.1	65	63.71	0.08	[0.083, 0.083]
		0.5	68	68.18	0.08	[0.08, 0.08]
		1.0	69	68.98	0.07	[0.079, 0.079]
	APPLAM	5.0	6	6.02	0.95	[0.948, 0.949]
		10.0	4	4.35	0.95	[0.946, 0.946]
		20.0	5	4.88	0.97	[0.964, 0.965]
8	Lamb	0.1	30	29.59	0.76	[0.764, 0.764]
		0.5	40	40.00	0.68	[1.0, 1.0]
		1.0	34	34.45	0.74	[0.738, 0.738]
	APPLAM	5.0	3	3.48	0.67	[0.658, 0.661]
		10.0	4	4.38	1.00	[0.993, 0.994]
		20.0	5	5.00	0.97	[0.972, 0.973]

Table 4: Simulation study B, $p = 100$: posterior modes and means of the number of clusters, the ARI between the estimated partition and the true one, credible intervals for the ARI between the random and true partition of the data with different values of the hyperparameters.

Latent dim	Model	Parameter	mode_nclus	avg_nclus	ari_best_clus	CI_aris
2	Lamb	0.1	9	8.45	0.88	[0.86, 0.861]
		0.5	9	9.03	0.88	[0.859, 0.86]
		1.0	9	9.44	0.88	[0.855, 0.856]
	APPLAM	5.0	8	7.90	0.69	[0.64, 0.647]
		10.0	7	6.87	0.61	[0.589, 0.594]
		20.0	7	7.23	0.69	[0.682, 0.684]
5	Lamb	0.1	8	8.22	0.97	[0.947, 0.949]
		0.5	75	75.26	0.06	[0.071, 0.071]
		1.0	76	76.42	0.07	[0.069, 0.069]
	APPLAM	5.0	4	4.47	0.95	[0.946, 0.947]
		10.0	6	5.90	0.91	[0.893, 0.897]
		20.0	5	4.73	0.93	[0.935, 0.936]
8	Lamb	0.1	61	60.44	0.16	[0.155, 0.155]
		0.5	62	61.59	0.13	[0.133, 0.133]
		1.0	61	60.54	0.16	[0.155, 0.155]
	APPLAM	5.0	4	4.07	0.96	[0.957, 0.958]
		10.0	4	4.00	0.97	[0.97, 0.971]
		20.0	4	4.00	0.99	[0.987, 0.987]

Table 5: Simulation study B, $p = 200$: posterior modes and means of the number of clusters, the ARI between the estimated partition and the true one, credible intervals for the ARI between the random and true partition of the data with different values of the hyperparameters

Latent dim	Model	Parameter	mode_nclus	avg_nclus	ari_best_clus	CI_aris
2	Lamb	0.1	9	9.72	0.87	[0.849, 0.851]
		0.5	11	10.81	0.85	[0.832, 0.834]
		1.0	11	11.29	0.84	[0.823, 0.825]
	APPLAM	5.0	6	6.52	0.46	[0.462, 0.464]
		10.0	12	13.04	0.63	[0.63, 0.633]
		20.0	7	6.91	0.46	[0.463, 0.465]
5	Lamb	0.1	8	8.17	0.97	[0.95, 0.951]
		0.5	8	8.32	0.97	[0.948, 0.95]
		1.0	91	91.02	0.05	[0.055, 0.055]
	APPLAM	5.0	6	6.35	0.92	[0.91, 0.911]
		10.0	6	5.82	0.91	[0.911, 0.913]
		20.0	5	5.15	0.91	[0.918, 0.919]
8	Lamb	0.1	77	78.12	0.09	[0.093, 0.094]
		0.5	75	75.02	0.11	[0.106, 0.106]
		1.0	84	83.47	0.08	[0.083, 0.083]
	APPLAM	5.0	4	4.01	0.97	[0.973, 0.973]
		10.0	5	4.73	0.95	[0.96, 0.961]
		20.0	4	4.07	0.97	[0.974, 0.975]

Table 6: Simulation study B, $p = 400$: posterior modes and means of the number of clusters, the ARI between the estimated partition and the true one, credible intervals for the ARI between the random and true partition of the data with different values of the hyperparameters.